



Cite this: *Soft Matter*, 2023,  
19, 2013

## Polyelectrolyte-multivalent molecule complexes: physicochemical properties and applications

Santiago E. Herrera,<sup>a</sup> Maximiliano L. Agazzi,<sup>\*b</sup> Eugenia Apuzzo,<sup>c</sup>  
M. Lorena Cortez,<sup>id c</sup> Waldemar A. Marmisollé,<sup>c</sup> Mario Tagliacruz<sup>a</sup> and  
Omar Azzaroni<sup>id \*c</sup>

The complexation of polyelectrolytes with other oppositely charged structures gives rise to a great variety of functional materials with potential applications in a wide spectrum of technological fields. Depending on the assembly conditions, polyelectrolyte complexes can acquire different macroscopic configurations such as dense precipitates, nanosized colloids and liquid coacervates. In the past 50 years, much progress has been achieved to understand the principles behind the phase separation induced by the interaction of two oppositely charged polyelectrolytes in aqueous solutions, especially for symmetric systems (systems in which both polyions have similar molecular weight and concentration). However, in recent years, the complexation of polyelectrolytes with alternative building blocks such as small charged molecules (multivalent inorganic species, oligopeptides, and oligoamines, among others) has gained attention in different areas. In this review, we discuss the physicochemical characteristics of the complexes formed by polyelectrolytes and multivalent small molecules, putting a special emphasis on their similarities with the well-known polycation–polyanion complexes. In addition, we analyze the potential of these complexes to act as versatile functional platforms in various technological fields, such as biomedicine and advanced materials engineering.

Received 16th November 2022,  
Accepted 10th February 2023

DOI: 10.1039/d2sm01507b

rsc.li/soft-matter-journal

### 1. Introduction

Since the pioneering work of Bungenberg de Jong at the beginning of the 20th century,<sup>1–4</sup> polyelectrolytes have been extensively studied from both experimental and theoretical points of view because they display distinct structural characteristics depending on the surrounding environment (solvent, pH, ionic strength, *etc.*).<sup>5</sup> There are several reasons for which polyelectrolytes are so appealing, and one of them is that many biologically relevant molecules are indeed polyelectrolytes. Plenty of theories have been developed to understand how this unique class of molecules behaves in solution, most of them with outstanding results. However, experimentalists are constantly defying the frontiers of what we think we understand by showing new and fascinating properties of complex-structured polyelectrolytes.

One of the simplest and, at the same time, most intriguing properties of polyelectrolytes is that they undergo phase separation in the presence of oppositely-charged polyelectrolytes.<sup>6</sup> The resulting product is known as a polyelectrolyte complex (PEC) (Fig. 1a). First studies on the complexation of polyelectrolytes can be traced back to 1910 when Tiebackx *et al.* studied mixtures of gelatin and gum arabic.<sup>7</sup> Later, Bungenberg de Jong expanded the understanding of the phase separation process using multiple polymers.<sup>4,8</sup> As their properties were being understood, PECs began to be applied technologically, especially in encapsulation of functional agents. In this context, it is worth to highlight the first commercial development patented by Green and Lowell in 1953 known as “Oil-containing microscopic capsules and method of making them”.<sup>9</sup> This invention was based on the design of gelatin and gum Arabic microcapsules loaded with ink oil and their surface deposition for the development of carbonless copying paper.

One of the simplest PEC system to study is the iconic poly(styrenesulfonate)/poly(diallyldimethylammonium chloride) (both strong polyelectrolytes) which is characterized by its structural simplicity and well known distribution of charges. For this system, Schlenoff and collaborators have demonstrated that phase separation is essentially driven by entropically-favorable counterions release and changes in water molecules distribution.<sup>10</sup> Furthermore, they showed that by regulating

<sup>a</sup> Departamento de Química Inorgánica, Analítica y Química Física, INQUIMAE, CONICET. Facultad de Ciencias Exactas y Naturales. Ciudad Universitaria, Pabellón 2, Buenos Aires C1428EHA, Argentina. E-mail: sherrera@qi.fcen.uba.ar

<sup>b</sup> Instituto para el Desarrollo Agroindustrial y de la Salud (IDAS), (UNRC, CONICET), Ruta Nacional 36 KM 601, 5800 Río Cuarto, Argentina. E-mail: magazzi@exa.unrc.edu.ar

<sup>c</sup> Instituto de Investigaciones Físicoquímicas Teóricas y Aplicadas (INIFTA), (UNLP, CONICET), Sucursal 4, Casilla de Correo 16, 1900 La Plata, Argentina. E-mail: omazzaroni@química.unlp.edu.ar

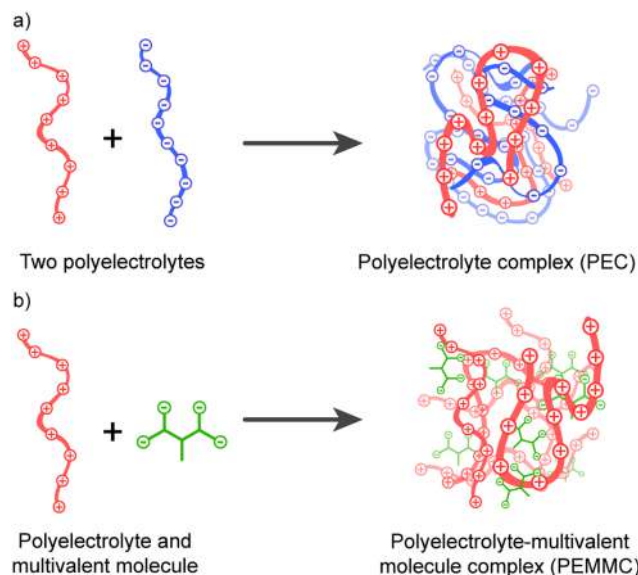


Fig. 1 Schematic representation of (a) the formation of a polyelectrolyte complex and (b) the formation of a polyelectrolyte-multivalent molecule complex.

the amount of KBr in the media, the association between polyelectrolytes can be tuned to give rise to different materials, spanning from solids to PEC-rich viscous liquids.<sup>11</sup> From this point we can identify two PEC systems with different rheological properties: solids, and highly viscous liquids named complex coacervates.<sup>11–13</sup>

Beyond Schlenoff findings, as the systems become more complex, other factors such as hydrophobic interactions, hydrogen bonding, short-range interactions, and functional groups-dependent interactions come into play, and the interplay between these factors ultimately define the characteristics of the condensed phase.<sup>10,14,15</sup> Since any highly-charged macromolecule can be considered as a polyelectrolyte, an extensive variety of PECs with different characteristics and features can be designed from diverse building blocks, such as synthetic polyelectrolytes, natural polyelectrolytes, surfactants, proteins, nucleic acids, and peptides, among others.<sup>16–24</sup>

As a general rule, macromolecular building blocks need to have enough electrostatic charges and to overcome a minimum molecular weight in order to condense into PECs.<sup>25</sup> Considering this last statement, which is the lower limit of molecular weight to form PECs? Polyelectrolytes are molecular chains containing charged monomers; therefore, we can consider a charged monomer as the smallest unit (*i.e.*, species with minimal molecular weight) that can undergo ion–ion complexation. In this framework, different studies have demonstrated that when a polyelectrolyte is mixed in aqueous solution with an oppositely charged multivalent molecule (*e.g.*, citrate ions), the system can also condense into PEC-like architectures (precipitates and complex coacervates).<sup>23,26–28</sup> Here we refer to “monovalent” and “multivalent” to denote the number of charges per ion. As literature is diffuse about the exact nomenclature of these special types of PECs, from now on we will call them polyelectrolyte-multivalent

molecule complexes, or PEMMCs (Fig. 1b). In PEMMCs, the forces that lead to phase separation appear to be similar to those for PECs; however, up to date, there are no exhaustive studies that correlate these two systems in a systematic way.

PEMMCs can be considered highly non-symmetrical systems as they are composed of two building blocks with markedly different molecular weights. In particular, at certain experimental conditions, PEMMC aggregates have a defined size within the nanometer scale (typically 200 nm) and remain relatively stable in colloidal dispersion (kinetically trapped state).<sup>26,29,30</sup> As well as PEC systems, PEMMC systems can form both precipitates and coacervates, therefore, a PEMMC nanometric aggregate can be strictly defined either as a nanoparticle or as a nanosized coacervate droplet. In many reports it is not clear whether the aggregate under study is solid or liquid since the macroscopic phase is not characterized in detail. Taking this into consideration, we will not distinguish between them and from now on we will call them PEMMC nanocomplexes.

In recent decades, PEMMC nanocomplexes have been intensively explored as nanocarriers of different payloads such as drugs, peptides, nucleic acids, proteins and medical imaging agents, among others.<sup>30,31</sup> Another advantage of PEMMCs, in contrast to other carriers, is their easy and fast preparation based on the simple mixing of building blocks under mild conditions (room temperature, atmospheric pressure, and aqueous solution). This methodology, generally called ionotropic (or ionic) gelation, was exploited by Calvo *et al.* in the late 90s representing one of the firsts all-aqueous alternatives to the water-in-oil technique.<sup>32</sup> In Calvo's work, the formation of colloidal PEMMCs nanocomplexes composed of chitosan and tripolyphosphate as well as their protein loading/release profiles were reported. Since this early report, the number of research articles using PEMMCs as drug delivery agents increased markedly, especially those based on chitosan/tripolyphosphate.<sup>33–37</sup> In the same manner as PECs, PEMMCs are highly sensitive to changes in the electrostatic interactions. The attenuation of these interactions can lead not only to swelling but also to a complete disassembly. This electrostatically-driven disassembly can be triggered by different external stimuli, making PEMMCs attractive for drug delivery and stimuli-triggered release applications.

In this review, we will begin by describing and analyzing the main physical-chemical fundamentals of conventional PECs, and then we will enter into the world of PEMMCs, from their properties and characteristics to their main technological applications.

## 2. Polyelectrolyte complexes

When mixing two (oppositely charged) polyelectrolytes in aqueous solution, an associative phase separation occurs, driven by cooperative electrostatic interactions and entropy changes due to counterion and water release. This gives as a result either a precipitate or a suspension of polymer-rich coacervate droplets.<sup>5,38,39</sup> While PEC precipitates consist of solid-like complexes with very low degree of hydration (Fig. 2a, picture

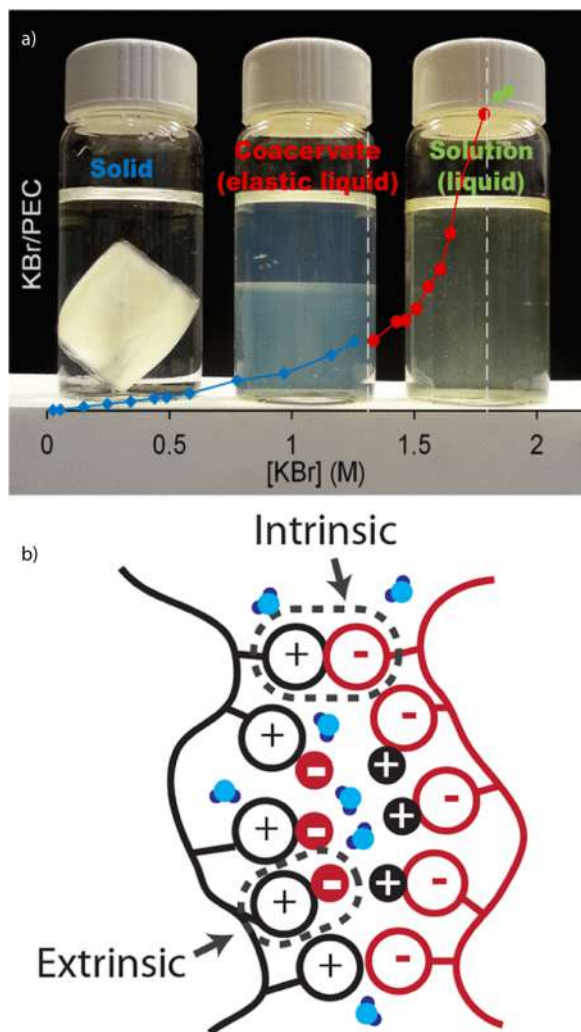


Fig. 2 When two oppositely-charged polyelectrolytes are combined in aqueous solution, a phase separation is produced. Depending on the nature of the polyelectrolyte backbones and the type and concentration of monovalent ions, the product of the phase separation can either be a solid or a liquid coacervate in coexistence with a solvent-rich supernatant phase (Reproduced with permission from ref. 11 Copyright (2014) American Chemical Society) (a). Independently of the macroscopic configuration obtained, the polymer-rich phase is generally called polyelectrolyte complex and it is composed of many polyelectrolyte chains interconnected by intrinsic and extrinsic ion pairs along with water molecules and salt counterions (Reproduced with permission from ref. 38 Copyright (2018) American Chemical Society) (b).

on the left), complex coacervates are condensed polymer-rich viscous liquids that are in coexistence with a second liquid phase made mostly by water (Fig. 2a, picture in the center).<sup>3</sup> Both types of configurations (solids and liquids) can not only be obtained from oppositely charged synthetic polyelectrolytes but also from peptides of different molecular weight, proteins, nucleic acids, and other charged macromolecules.<sup>40–44</sup> Usually, while coacervates are more prone to form in the presence of moderate ionic strength ( $\sim 500$  mM NaCl), precipitates are commonly observed in the absence of added salt.<sup>11,45–47</sup> Although this rule applies in many cases, the rheological properties of the condensed phase (solid or liquid) will be dictated in ultimate state by a

delicate combination of soft interactions. In this regard, Vieregg *et al.* demonstrated that while poly-L-lysine tend to form fluid coacervates with single-stranded DNA, the combination of the same polypeptide with double-stranded DNA conducts to solid-like materials.<sup>48</sup> Here, the main cause for the phenomenon was ascribed to differences in DNA charge density. In another example, Perry *et al.* showed that polylysine/poly(glutamic acid) mixtures formed precipitates or coacervates depending on whether polyaminoacids were chiral or racemic, respectively.<sup>49</sup> In this case, the formation of hydrogen-bonding networks in PECs obtained from chiral polyaminoacids was demonstrated to be the main cause for the difference observed. So, subtle changes in polyelectrolyte's backbones can lead to dramatic changes in the viscosity of the PEC (the viscoelastic characteristics of PECs cannot be predicted before mixing of components).

Complex coacervate systems own the unique characteristic of having an extremely low interfacial tension between polymer-rich and polymer-depleted phases ( $\sim 100\text{--}1000$   $\mu\text{N m}^{-1}$ ),<sup>50–52</sup> a phenomenon that was recently ascribed to the formation of a bicontinuous and biphasic nanostructured fluid network of polyelectrolytes complexes and water with a very weak cohesive energy between them.<sup>53</sup> The low interfacial tension property of complex coacervates also applies to interfaces between coacervates and a large number of solid surfaces, and is particularly relevant when complex coacervate phases are brought into contact with solid surfaces and high-salt water solutions. We encourage readers to go deeper into issues related to the interfacial tension of complex coacervates and its impact on many technological applications by consulting the review article written by Dong Soo Hwang.<sup>54</sup>

Without considering non-electrostatic effects, the microscopic structure of PECs in general (whether it forms a solid precipitate or a complex coacervate) can be described by a combination of two different types of ion pairs: intrinsic and extrinsic. While intrinsic ion pairs establish between charged polymer groups, extrinsic ion pairs form between unbound charged polymer groups and small counterions (Fig. 2b).<sup>55</sup> An increase in the concentration of salt forces the intrinsic ion pairs to disrupt and to become extrinsic ion pairs, destabilizing the whole structure. This is the main reason why PECs can be disassembled at an elevated ionic strength (see Fig. 2a, picture on the right). Lutkenhaus and coworkers elucidated that the molar ratio between water molecules and intrinsic ion pairs ( $n_{\text{H}_2\text{O}}/n_{\text{intrinsic ion pair}}$ ) correlates with the material's glass transition temperature  $T_g$ , independently of the chemical identity of the polyelectrolytes, the type of assembly method, and even the concentration of salt (eqn (1)).<sup>55</sup> Therefore, water molecules act as PEC plasticizers by weakening intrinsic ion pairing and changing the rheological properties of the material.<sup>56</sup>

$$\frac{1}{T_g} \sim \ln\left(\frac{n_{\text{H}_2\text{O}}}{n_{\text{intrinsic ion pair}}}\right) \quad (1)$$

### 2.1. Stoichiometric polyelectrolyte complexes

The phase behavior and the influence of salt ions in PECs is often studied by constructing the so-called binodal phase

diagrams in stoichiometric conditions (1:1 stoichiometric ratio of charge-matched conditions).<sup>57,58</sup> These diagrams are obtained by mixing oppositely-charged polyelectrolytes having the same number of charges per molecule and final concentration (*i.e.*, polyelectrolyte charges are present in stoichiometric amounts) at different concentrations of monovalent salt. In the conditions where the system undergoes phase separation, the total concentration of polyelectrolytes and the salt in each phase is measured. For each initial salt and polyelectrolyte concentration, a pair of points is plotted in the diagram indicating the concentration of components in each phase, see Fig. 3. While points with high polyelectrolyte concentration correspond to the polyelectrolyte-rich phase, points with low polyelectrolyte concentration correspond to the water-rich phase. The salt concentration required to unify the polymer-rich and the water-rich branches is known as the critical point. On the other hand, the salt concentration needed to dissociate the PEC (*e.g.*, the salt concentration needed to leave the two-phase region) is generally called salt resistance, and depends on the initial concentration of polymer (the maximum salt resistance is observed at the critical point).<sup>59,60</sup> As we mentioned, any given system within the two-phase region results in two coexisting phases. The points indicating the concentrations of the initial system and the coexisting phases are connected by a tie line. While a tie line with a slope of 0 indicates that salt ions distribute equally between the two phases, a negative slope is indicative of a salt partitioning into the water-rich phase, and a positive slope is indicative of a salt partitioning into the polyelectrolyte-rich phase.<sup>58</sup> Note that all

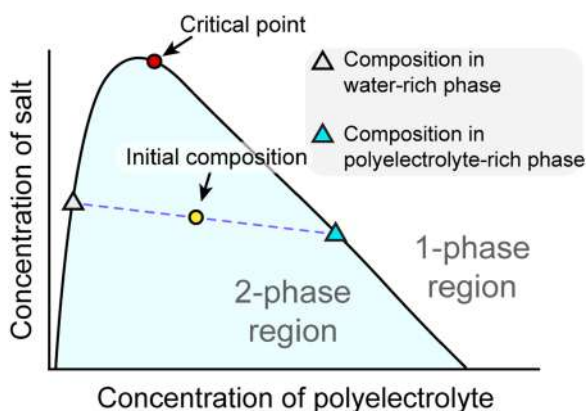


Fig. 3 Schematic representation of the binodal phase diagram of a mixture of oppositely-charged polyelectrolytes in aqueous solution under charge and length matching conditions. The abscissa corresponds to the total concentration of polyelectrolyte (polyanion + polycation) and the ordinate to the concentration of monovalent salts. Each point within the two-phase region (highlighted in light-blue) corresponds to a system that separates into two phases: a polymer-rich and a water-rich phase. The violet dashed line (tie line) connects the compositions of the two coexisting phases after separation (triangles). The initial composition of the system is shown with a yellow dot. The point where the polymer-rich and the water-rich branches connect (red dot) is known as the critical point. The critical point is independent of the initial polymer concentration and does not coincide with the maximum of the binodal as tie lines are not horizontal.

initial systems lying on the same tie line will produce the same two coexisting phases. The relative amount of each of these coexisting phases is given by the lever rule.

In this regard, Tirrell's group constructed binodal phase diagrams for PEC systems composed of polyelectrolytes of different length and backbone hydrophilicity.<sup>61,62</sup> For studying the effect of the polyelectrolyte length, the system chosen was (poly(L-lysine hydrochloride)/poly(D,L-glutamic acid))<sub>N</sub> (PLK/PRE), with *N* = 20, 50 and 400 the length of PLK and PRE chains (polyelectrolytes chemical structures are displayed in Fig. 4a). As shown in Fig. 4b, the two-phase region in binodal phase diagrams became bigger as *N* increased, in concordance with previous findings.<sup>57</sup> Also, the salt resistance increased in the same way. These findings can be explained in terms of increasing cooperative electrostatic interactions and larger entropy gains from counterion release that scale with the chain length of polyelectrolytes. To study the solvent-to-polyelectrolyte interaction effect, four different PEC systems with increasing hydrophilic characteristics were tested: poly(allylamine)/poly(acrylic acid) (PAH/PAA), PAH/PRE, PLK/PAA, and PLK/PRE (Fig. 4a). As a first observation, while hydrophilic pairs formed liquid complex coacervates, hydrophobic pairs conducted to amorphous precipitates or semisolid soft structures, depending on the concentration of salt. This indicates that, depending on the hydrophilicity of the polyelectrolyte backbone, the water content in the polyelectrolyte-rich phase varies. As mentioned before, the variations in the rheological characteristics of PECs are tied to the amount of water molecules surrounding intrinsic ion pairs. Then, hydrophobic interactions would produce a depletion in the hydration sphere of intrinsic polyelectrolyte ion pairs. In agreement with this observation, binodal phase diagrams in Fig. 4c show an increase in both the two-phase region area and the salt resistance as polyelectrolytes become more hydrophobic (note that the critical point is not reachable for the PAH/PAA system). These results point out that the cohesion and the water content in polymer-rich phases are highly dependent on the solvent quality.<sup>62,63</sup>

Complex coacervation was also studied theoretically.<sup>64,65</sup> The first model that was able to phenomenologically capture the phase behavior of complex coacervates is the Voorn–Overbeek theory.<sup>66,67</sup> Essentially, the Voorn–Overbeek theory describes the mixing free energy of the system as a combination of the translational entropy within the Flory–Huggins theory framework, and the electrostatic attraction using the Debye–Hückel theory. The original Voorn–Overbeek theory didn't account for the possible contribution of short-range (van der Waals) forces to the energy of mixing, therefore, a third contribution is usually added to the energy expression that includes the short-range interactions in terms of the Flory  $\chi$ -parameter.<sup>68</sup> The free energy (*F*) of the system can thus be written as:

$$\frac{a^3 F}{VkT} = \sum_i \frac{\phi_i}{N_i} \ln(\phi_i) - \alpha \left[ \sum_i \sigma_i \phi_i \right]^{\frac{3}{2}} + \sum_i \sum_{j>i} \chi_{ij} \phi_i \phi_j \quad (2)$$

with *V* the total volume, *a* the size of the charged monomer, *kT* the thermal energy,  $\phi_i$  the volume fraction of component *i* (*i* = +, −, P+, P−, S), *N<sub>i</sub>* the chain length of component *i*,  $\sigma_i$  the charge

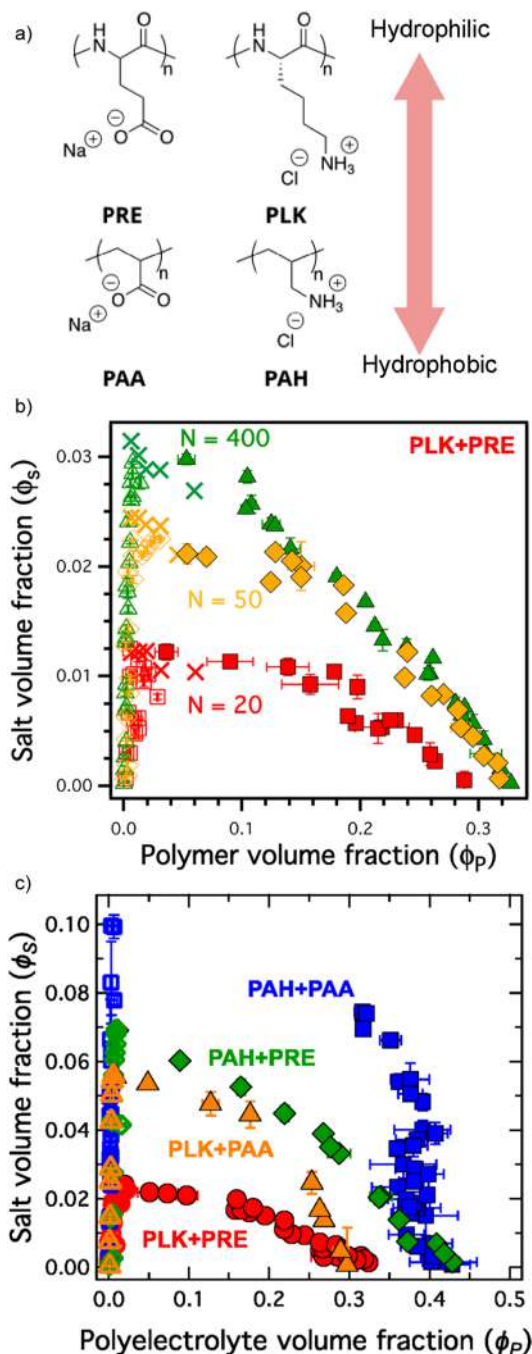


**Fig. 4** (a) Structures of poly-D,L-glutamic acid sodium salt (PRE), poly(L-lysine hydrochloride) (PLK), poly(sodium acrylate) (PAA), and poly(allylamine hydrochloride) (PAH). While the first two have a hydrophilic backbone, the second two have a hydrophobic backbone. These polyelectrolytes give four different PEC systems with different hydrophilicity. (b) Experimental binodal phase diagrams for a PLK/PRE PEC system with fixed initial polymer concentration and different chain lengths  $N = 20$  (red symbols), 50 (orange symbols) and 200 (green symbols). Reproduced with permission from ref. 61 Copyright (2018) American Chemical Society. (c) Experimental binodal phase diagrams for the four possible systems with fixed length and polymer concentration: PLK/PRE (red symbols), PLK/PAA (orange symbols), PAH/PRE (green symbols), and PAH/PAA (blue symbols). In both phase diagrams, filled symbols correspond to compositions of the system in the polymer-rich phase, and empty symbols correspond to the water-rich phase. Each pair of points correspond to the phase separation of an initial solution with a given amount of added salt. Phase diagrams are expressed in terms of volume fractions instead of molar concentrations. Reproduced with permission from ref. 62 Copyright (2021) American Chemical Society.

density of component  $i$ ,  $\chi_{ij}$  the Flory  $\chi$ -parameter between each pair of species  $i$  and  $j$ , and  $\alpha$  the electrostatic interaction parameter. To build the binodal curve using the Voorn–Overbeek theory, one must find the concentrations of the two coexisting phases (polymer-rich  $\alpha$  phase and polymer-depleted  $\beta$  phase), so that the chemical potentials of all species are equal in both phases ( $\mu_i^\alpha = \mu_i^\beta$ ). Although eqn (2) was used to fit experimental data successfully,<sup>57,69</sup> it was demonstrated that the model provides a poor description of the PEC formation process.<sup>70,71</sup> For example, the Voorn–Overbeek theory predicts tie lines with positive slopes (salt partitioning in the polymer-rich phase) as the model assumes that the condensation is an enthalpy-driven process due to electrostatic attraction between species (a fact that was experimentally contradicted by Fu and Shlenoff). By means of a highly reproducible method, Tirrell *et al.* have demonstrated that tie lines in PAH/PAA phase diagrams usually present negative slopes, independently of the working pH.<sup>14</sup> In another report, a combination of experimental and simulation approaches was used to determine the cause of the salt enrichment in the diluted phase.<sup>61</sup> Here, excluded volume interactions between species was found to be the main reason why counterions tend to be expelled from the polymer-rich phase into the water-rich phase, a contribution that was not considered in the earliest studies of Voorn and Overbeek. In this way, the Voorn–Overbeek theory is currently considered just as a simple approach that phenomenologically describes complex coacervation rather than a predictive theory. More refined theoretical treatments include: the polymer field theory, the scaling theory, the counterion release models, the random phase approximation approach, the field theory approach, the chemical-equilibrium formalism and the simulation approach.<sup>72–74</sup> A deep insight into these theories can be found in the two excellent review articles written by Charles Sing where a complete description of the latest advances in the field is made.<sup>70,71</sup>

## 2.2. Non-stoichiometric polyelectrolyte complexes

Usually, PEC's phase behavior is studied under stoichiometric conditions. This means that all polycations and polyanions complex each other, fully neutralizing their charges. When dealing with strong polyelectrolytes, it is easy to construct stoichiometric PECs, as the concentration of charges scales linearly with the monomeric concentration. On the other hand, weak polyelectrolytes are more complicated to study, as their charge degree varies with the pH. In this case, a common strategy to study phase behavior is to work at a certain pH at which both polyanion and polycation are equally charged ( $\text{pH} = \frac{\text{p}K_{a \text{ pol } A} + \text{p}K_{a \text{ pol } B}}{2}$ ). The scenario in which polyelectrolytes are charge-matched rarely occurs in real systems where both relative concentrations and charge degrees do not match. Next, we will discuss some particularities of PEC systems where concentrations of each polyelectrolyte are not coincident.

According to the Voorn–Overbeek theory, a four-component system (polycation, polyanion, monovalent salt and water) will display a three-dimensional phase diagram which can be reduced to a two-dimensional phase diagram when the

concentration of salt is fixed. Fig. 5a shows the binodal phase diagram for a non-stoichiometric system at different salt concentrations, assuming that salt ions partition equally in both phases. As a first observation, we can see that the two-phase region gets narrower as the concentration of salt increases. Eventually, when the concentration of salt becomes larger than the salt resistance, the two-phase region disappears. For a 1 : 1 stoichiometric ratio situation, the compositions in the water- and polyelectrolyte-rich phases will likely also be stoichiometric (see the tie line crossing the origin in Fig. 5a). When one of the polyelectrolytes is in excess (*i.e.*, point in the  $xy$  plane within the

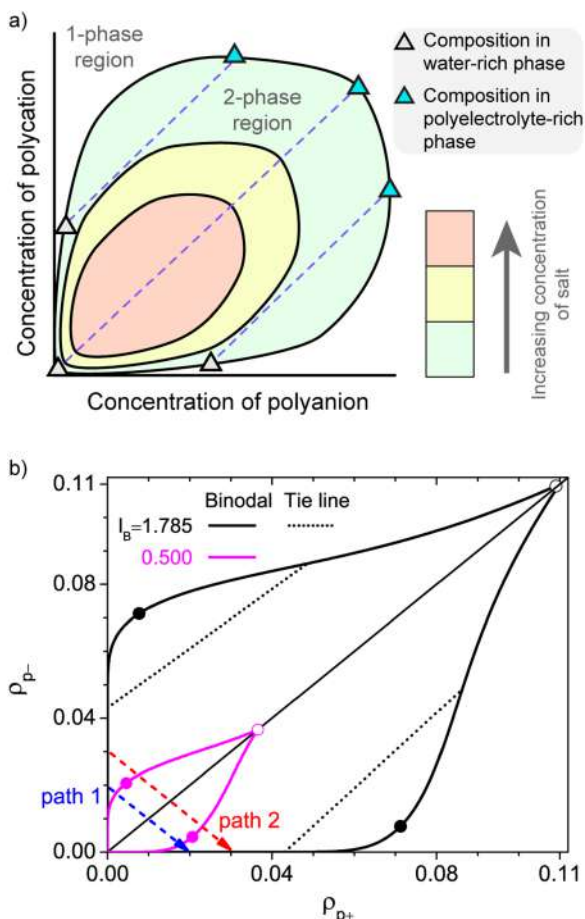


Fig. 5 Binodal phase diagrams for non-stoichiometric mixtures of oppositely-charged polyelectrolytes (asymmetric PECs). (a) Schematic representation of the binodal phase diagram with a closed-loop shape at fixed concentration of monovalent salts. The plot shows the overlap of three phase diagrams at three different concentrations of monovalent salt. At high salt concentration, the two-phase region shrinks until it disappears. For an initial composition inside the two-phase region, the system will phase-separate and the compositions of each phase will be determined by the crossing between the closed-loop binodal and a tie line (violet dashed line). (b) Overlap of two binodal phase diagrams with two different Bjerrum lengths ( $l_B$ ) in the  $\rho_{p+}$  (concentration of polycation) –  $\rho_{p-}$  (concentration of polyanion) plane at fixed concentration of monovalent ions, calculated by Zhen-Gang Wang using the liquid-state theory. Here, the critical points where both the polymer-rich and the water-rich branches connect are marked with black dots. Reproduced with permission from ref. 77 Copyright (2018) AIP Publishing.

two-phase region and not coincident with the stoichiometric line), the compositions of the two phases will be determined by the intersections between a line parallel to the stoichiometric line and the curve of the binodal phase diagram (tie lines are not necessarily parallel to the stoichiometric line in real systems).<sup>75</sup> As PECs are ruled by electroneutrality, the phase separation in non-stoichiometric mixtures will involve the exchange of monovalent counterions from one phase to the other. When one of the components is in large excess, the entropic cost for the exchange of monovalent ions is too large and the system does not phase-separate. Therefore, starting with an aqueous solution of a given polyelectrolyte, PECs can be formed and then re-dissolved by simply adding increasing concentrations of an oppositely charged polyelectrolyte (reentrant condensation). It is worth mentioning that the phase diagram depicted in Fig. 5a is just a schematic representation. A more realistic picture of the complex coacervate phase diagram at non-stoichiometric conditions can be found in the works of Sing and Wang.<sup>76,77</sup>

Zhen-Gang Wang introduced a simple liquid-state theory to study the precipitation of single-polyelectrolyte solutions in the presence of monovalent salts (*i.e.*, aqueous solutions of polyvinyl-sulfonic acid separate into two liquid phases at high concentrations of added monovalent electrolytes).<sup>78</sup> The liquid-state theory developed by Wang assumes that the phase separation is driven purely by electrostatic correlations and gives an expression for the Helmholtz free energy with four contributions: the translational entropy of each component, the hard-core excluded-volume repulsion (using the Boublik–Mansoori–Carnahan–Starling–Leland equation of state), the electrostatic correlations (described by the mean-spherical approximation), and the excess Helmholtz free energy due to chain connectivity (in terms of the first-order thermodynamic perturbation theory).<sup>79</sup> The incorporation of the chain connectivity term was found to have a profound effect in the salt partitioning of symmetric complex coacervates.<sup>80</sup> By equalizing the chemical potentials of all species and equalizing the osmotic pressure of both phases (polyelectrolyte-rich and polyelectrolyte-poor phases), a closed-loop binodal phase diagram was obtained using the liquid-state theory for the system polyelectrolyte-salt, in good agreement with experiments. Later on, Wang extended the liquid-state theory to a 4-component system (polycation, polyanion, small cation and small anion), and studied the phase behavior of PECs under non-stoichiometric conditions.<sup>77</sup> As a result, a three dimensional phase diagram was obtained in the  $\rho_{p+}$  (concentration of polycation) –  $\rho_{p-}$  (concentration of polyanion) –  $\rho_{p+}$  (concentration of small cations) space at fixed Bjerrum length  $l_B$  (the length at which the electrostatic interaction between two unit charges in the dielectric continuum is equal to the thermal energy). Then, by intercepting the phase diagram with the plane  $\rho_+$  (*i.e.*, salt-free non-stoichiometric mixtures), the two-dimensional binodal phase diagram depicted in Fig. 5b was obtained. As shown in this plot, the liquid-state theory predicted parallel tie lines and a two-phase region that reduces for decreasing  $l_B$ . Moreover, if  $l_B$  is low enough, the two-phase region disappears.<sup>77</sup> Also, an interesting result was obtained when studying the titration of the polyanion with the polycation, which correspond to a path that starts on the ordinate

and ends on the abscissa in a direction perpendicular to the diagonal line (see paths denoted by arrows in Fig. 5b). The model predicts that, depending if the path is over or below the critical point (see solid circles in Fig. 5b), it is the polyelectrolyte-rich or the polyelectrolyte-poor phase that first appears. In other words, when the system separates in phases,

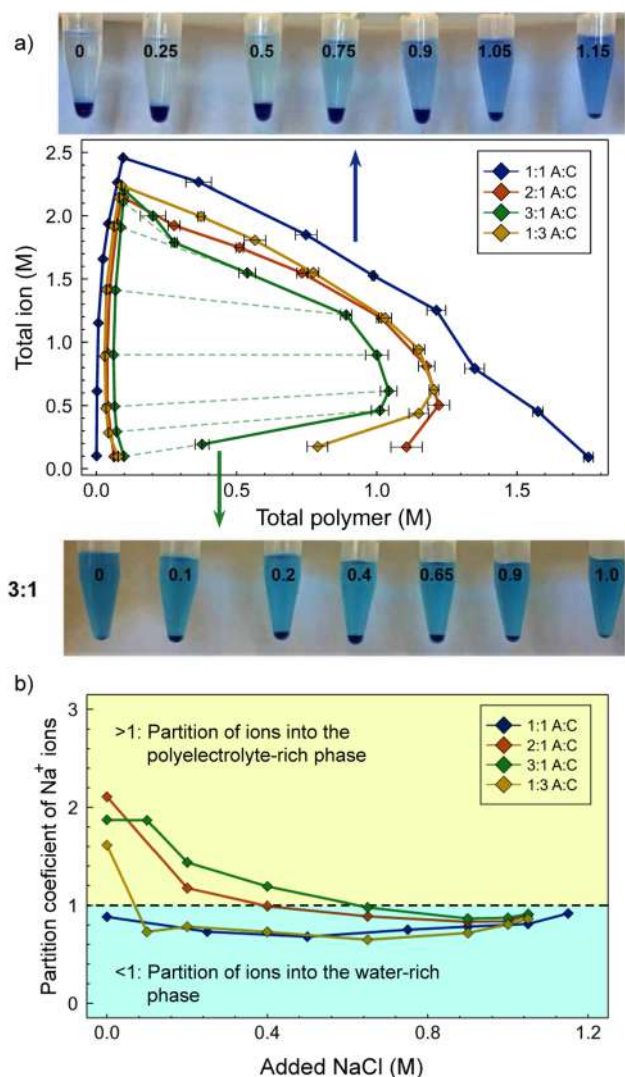


Fig. 6 Experimental phase diagrams of a PEC system under non-stoichiometric conditions. (a) The blue curve corresponds to a symmetrical system on which both the polyanion (A) and the polycation (C) are mixed in equal concentrations and with different amounts of added monovalent salt. The pictures in the upper panel show the different samples after phase-separation (the number over each sample tube denotes the concentration of monovalent salt). Red, green and orange curves correspond to asymmetric systems with different initial polyanion:polycation mixing molar ratios. The green curve (3:1 A:C) displays a closed-loop shape at low salt-concentrations. The lower picture shows the different 3:1 samples after phase-separation. (b) Analysis of the  $\text{Na}^+$  partitioning for each system investigated in (a). Note that, while in the stoichiometric mixture salt ions tend to concentrate in the supernatant phase, in non-stoichiometric mixtures salt ions concentrate in the polymer-rich phase at low salt concentrations (tie lines with positive slopes). Reproduced with permission from ref. 81 Copyright (2021) AAAS.

the volume fraction of each phase is highly dependent on the path that was used to perform the titration. This is a non-trivial result since in many real systems the relative volume fraction of coacervates can be a determining factor.

Although progress has been made in the area of computational physical chemistry,<sup>76,77</sup> there is a lack of experimental approaches that focus on non-stoichiometric PEC systems. In this context, Qin and coworkers made a major contribution by studying the effect of non-stoichiometry of a PEC system composed of fluorescent-labeled polyacrylamides with pendant ammonium or sulfate groups with equal chain lengths and charge densities.<sup>81</sup> By UV-Vis spectroscopy and ICP-MS measurements, they were able to quantify polyelectrolytes and salt concentrations, constructing binodal phase diagrams of non-stoichiometric polyelectrolyte mixtures. Fig. 6a shows the binodal phase diagrams for mixtures with a total polymer concentration of 0.1 M and different molar ratios A:C, where A is the polyanion and C is the polycation. At low salt concentration, there is a salting out effect, in which the addition of salt triggers the formation of the coacervate. Also, tie lines in the low-salt regime have a positive slope indicating a preferential partitioning of monovalent ions into the complex coacervate (see Fig. 6b). After certain concentrations of salt, all non-stoichiometric systems recovered the usual trends observed for 1:1 mixtures. The anti-intuitive salting-out effect at low salt concentrations was explained in terms of a competition of the mixing entropy of counterions and the electroneutrality constraint in the coacervate. A similar argument is used to explain that coacervates do not form when concentration asymmetry is too high.

### 3. Polyelectrolyte-multivalent molecule complexes

PEMMCs result from the interaction between polyelectrolyte chains and multivalent small molecules with opposite charge in aqueous solution, as depicted in Fig. 7.<sup>30,31</sup> When we refer to “multivalent small molecules”, we mean molecules such as phosphate, pyrophosphate, tripolyphosphate, citrate, and even larger molecules such as oligoamines and modified sugars. In this review article we will exclude multivalent metal cations, such as  $\text{Ba}^{2+}$ ,  $\text{Ca}^{2+}$ ,  $\text{La}^{3+}$ , *etc.*, from the definition of multivalent small molecule, however, the basic principles discussed could be applied to study these ions.<sup>82</sup> On the other hand, small peptides bearing charged aminoacids can also be considered as multivalent small molecules. However, it is difficult to establish a weight limit (or a chain length limit) at which a small peptide is considered a macromolecule. Therefore, and as a general rule for this review article, we consider a multivalent small molecule to be any molecule with more than 1 charge and less than 10 charges. As well as PECs, PEMMCs condense into different physical states. Depending on the balance of weak interactions between constituents, PEMMCs can be obtained in form of precipitates, fluid coacervates, rubbery-like viscoelastic materials, and water-rich gels.

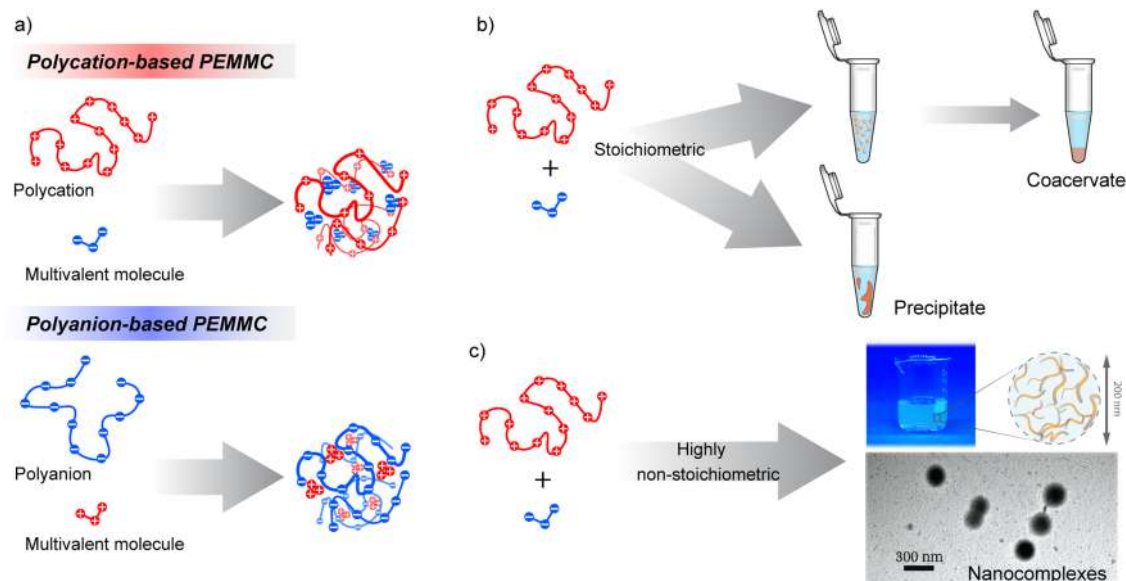


**Fig. 7** PEMMCs result from the phase-separation of a polyelectrolyte and an oppositely-charged multivalent small molecule in aqueous solution (a). In a similar way to PEC systems, PEMMCs are composed of polyelectrolytes and multivalent molecules that interconnect together by ion pairing. Depending on the initial composition, the system can transition into macroscopic liquid coacervates, dense precipitates, or dispersed nanocomplexes (here we do not distinguish between nanometric liquid-like coacervate droplets and solid-like nanocomplexes). Generally, while stoichiometric mixtures (equal number of positive and negative charges) give rise to coacervates and precipitates (b), non-stoichiometric mixtures condense into nanocomplexes (c).

As polyelectrolytes can be polyanions or polycations, PEMMCs can be either based on polyanions (adding a multivalent cationic molecule),<sup>83</sup> or polycations (adding a multivalent anionic molecule).<sup>84</sup> During the process of PEMMC formation, and in a similar fashion to PEC formation, multivalent molecules first interact with polyelectrolyte monomers, expelling their counterions and establishing bridges between neighboring chains.<sup>85</sup> As this process goes along, more polyelectrolyte chains are incorporated into the core structure, driven by ion pairing with multivalent molecules. Under near stoichiometric charge mixing conditions, PEMMCs phase-separate into precipitates or coacervates, which suggests that the physical chemistry underlying the formation of PEMMCs is somehow similar to that of the formation of PECs.<sup>86,87</sup> In this regard, PEMMCs condense into either precipitates or coacervates depending primarily on their specific molecular interactions and not only on electrostatic effects.<sup>25</sup>

On the other hand, if the concentration of charges associated with the multivalent molecule is less than the concentration of charges associated with the polyelectrolyte (non-stoichiometric conditions), the aggregation process results in the formation of clusters that are superficially charged.<sup>88</sup> While the first stage of PEMMC formation is very fast and occurs in the range of seconds, a further slower size-increasing regime takes place, dominated by coalescence or precipitation in a similar way to the formation process of PEC coacervates or precipitates.<sup>29,85</sup> Under specific experimental conditions (highly non-stoichiometric), PEMMCs aggregates display a defined size in the range of a few hundred nanometers and remain relatively stable (do not undergo precipitation) in colloidal suspension (PEMMC nanocomplexes).<sup>33,34,89–94</sup> Here, it is important to remark that in all PEMMC systems the thermodynamically stable phase is

the macroscopic phase. Therefore, a suspension of PEMMC nanocomplexes can be thought as a system that is kinetically trapped.<sup>95,96</sup> In order to produce a stable dispersion of PEMMC nanocomplexes, the surface charge must be maximized and the van der Waals interactions between pairs of colloids must be minimized. In other words, it is accepted that most PEMMC formulations respond to the Derjaguin, Landau, Verwey, and Overbeek (DLVO) theory.<sup>67</sup>

### 3.1. PEMMC building blocks

The main condition to produce a PEMMC aggregate (or coacervate) is to have a sufficiently charged polyelectrolyte (independently of its chemical structure) and a molecule with high enough charge. This is the reason why PEMMCs are so versatile. Depending on the hydrophobicity of the selected polymer and multivalent molecule, there will be a restriction on the minimum valency for the system to induce phase-separation. Experimentally, it is observed that the more hydrophilic the building are, the higher the valency required for phase separation (and *vice versa*).

For example, using molecules with  $z = -2$  such as succinate, hydroxysuccinate and sulfate, Wong *et al.* showed that PEMMCs were successfully formed in the presence of poly(allylamine) (a polyelectrolyte with a highly hydrophobic backbone) but not in the presence of poly(L-lysine) (with a more hydrophilic backbone).<sup>26,29</sup> Furthermore, McKenna *et al.* were able to complex different positively charged polyaminoacids (hydrophilic backbone) using molecules with  $z = -3$  such as citrate, isocitrate and trimesate, but failed to do it with divalent molecules.<sup>97</sup> In another example, when using chitosan as polycation (a highly hydrophilic biopolyelectrolyte), citrate ( $z = -3$ )

do not produced a phase separation and a more charged anion like tripolyphosphate ( $z = -5$ ) was needed to form PEMMCs.<sup>98</sup> This evidence suggests that, although electrostatics are surely needed to drive the phase separation, the entropy variation due to water molecule rearrangements can also be determining. Another key factor that may be responsible for the trends observed is the linear charge density of the polyelectrolyte. In all cases mentioned before, the more densely charged is the polyelectrolyte, the less is the charge needed for the multivalent molecule to produce the phase separation, and *vice versa*. More specifically, while PAH is a linear polyelectrolyte bearing one charge every second backbone atom (in their fully charge state), polyaminoacids and chitosan display charges that are less densely accommodated within the polymeric backbone. The linear charge density of the macromolecule could then have an impact on the spatial ion pairing between polyelectrolyte chains and multivalent molecules, promoting (or preventing) the interaction with less charged molecules.

It was also shown that the hydrophilicity of the small molecule can determine whether PEMMCs will form or will not. Several reports indicate that low net charge (+1 or -1) hydrophobic bioactive molecules (including vancomycin, itraconazole, ciprofloxacin, ofloxacin, levofloxacin, ibuprofen, curcumin, perphenazine, amphotericin B, and doxorubicin) are able to act as crosslinkers of biodegradable hydrophilic polymers such as dextran, carboxymethyl cellulose, chitosan, polyglutamic acid, and carrageenan, among others.<sup>21,99–105</sup> This special type of PEMMC in which hydrophobic effects are dominant (known in the literature as nanoplexes) is usually employed as a dual-function system as they both increase the solubility of hydrophobic biomolecules and act as nanocarriers for therapeutic treatments.<sup>106–108</sup>

Regarding the rheological properties of the macroscopic phase, it was recently reported that the viscoelastic response of a PEMMC can change dramatically with the valency of the molecule. More specifically, Schlenoff *et al.* analyzed the viscoelastic response of the product of complexation between poly(diallyldimethylammonium) and a series of hydrophobic molecules bearing from one to four sulfonates each.<sup>109</sup> Using large-scale rheological measurements, it was found that, by increasing the charge of the multivalent molecule from three to four, the viscosity increased 160 times and the complex phase changed from liquid to rubbery. The latter, very similar to a typical PEC system.

### 3.2. Effect of monovalent ions

At this point, it is clear that PEMMCs can be treated as a special case of PECs. The reason why it is so, is that PEMMCs can be considered as complexes formed by interaction between a long-chain polyion and a short-chain polyion.<sup>88,110</sup> In other words, the system is, essentially, a highly asymmetric PEC. It is not surprising, then, that PEMMCs had the tendency to dissolve at elevated ionic strength solutions. Therefore, for a given polymer concentration, there will be a given amount of monovalent salt necessary to dissolve the PEMMC (salt resistance). In a recent report, Spruijt *et al.* synthesized PEMMCs coacervates based on oligoarginine (poly-L-arginine hydrochloride with

10 residues) and different multivalent small molecules such as carboxylic acids, phosphate group-containing molecules, sulfate group-containing molecules, and iron hexacyano complexes.<sup>87</sup> Here, they evaluated the salt resistance of each PEMMC (here referred to as critical salt concentration), and found that the salt resistance increases with the valence of the small molecules (Fig. 8a). In another approach, the same authors determined the salt resistance for the systems ATP/poly-L-lysine and ADP/poly-L-lysine at fixed polymer concentration and variable multivalent molecule concentration, and found that the salt resistance was always higher for the more charged ATP ion (Fig. 8b).<sup>111</sup> The same trend was observed when forming complex coacervates of  $\text{Fe}(\text{CN})_6^{4-}$ /Poly-L-lysine and  $\text{Fe}(\text{CN})_6^{3-}$ /Poly-L-lysine.<sup>112</sup> As it can be observed in Fig. 3,

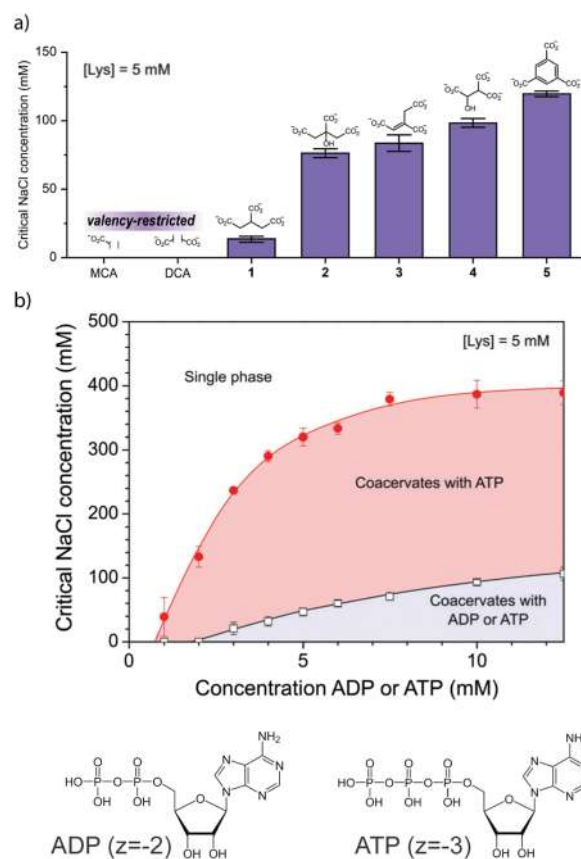


**Fig. 8** (a) Salt resistance (concentration of salt needed to dissolve the complex) of PEMMC systems composed of poly-L-lysine (5 mM, monomer) and various multivalent small molecules. Molecular structures are displayed over bars. Note that when molecules with  $z = -1$  and  $z = -2$  are used to form PEMMC with poly-L-lysine, the salt resistance is zero. This indicates that these systems do not phase-separate (there is a valency restriction). Reproduced with permission from ref. 87 Copyright (2022) Wiley-VCH Verlag GmbH & Co. (b) Evaluation of the salt resistance as a function of the concentration of multivalent molecules for two systems: poly-L-lysine/ADP ( $z = -2$ ) and poly-L-lysine/ATP ( $z = -3$ ) (molecular structures of ADP and ATP are displayed below). The red area corresponds to a region of concentrations on which the system phase separates for ATP but not for ADP. The gray area corresponds to a region of concentrations on which the system phase separates for both ATP and ADP. Reproduced with permission from ref. 111 Copyright (2018) Royal Society of Chemistry.

the salt resistance of a stoichiometric mixture of polyelectrolytes has a maximum. On the other hand, when dealing with non-stoichiometric mixtures, the salt resistance can be more difficult to predict (see phase diagram on Fig. 5). Although it was observed an increase in the salt resistance with the valency in PEMMC systems, it is not trivial to extend this result to all PEMMC systems. A change in valency implies a change in stoichiometry. Therefore, the phase behavior should change with the concomitant change of the salt resistance. Unfortunately, there are no exhaustive studies that focus on the salt resistance of different PEMMCs under stoichiometric conditions. Most likely, however, the response of PEMMC to monovalent salts is similar to that of PEC.

Another interesting effect of monovalent salts on PEMMCs is that they cause a decrease in the cooperative ionization that takes place on weak polyelectrolytes during complexation. Cooperative ionization is the tendency of a molecule to acquire charge in the presence of another molecule, driven by electrostatic interactions.<sup>113–117</sup> When working with weak acids and bases, this phenomenon is detected by a shift in the pKa of species. For example, when mixing poly(allylamine) and phosphate ions in absence of added monovalent salts at pH = 8, the formation of PEMMC led to the cooperative ionization of the polymer (the polymer takes protons from the media) and the pH of the solution increases up to 9.2. The addition of 0.2 M of KCl produces the partial suppression of the cooperative ionization and the pH goes back to the initial value.<sup>84</sup>

### 3.3. Reentrant condensation of PEMMCs

In many PEMMCs the increment in the multivalent molecule concentration can firstly induce phase separation but then allow for the complete resolubilization at high enough concentration. This effect has been referred to as reentrant condensation. At very low concentration of multivalent molecules, former monovalent counterions begin to be replaced by multivalent counterions as depicted in Fig. 9a.<sup>26</sup> At this stage, soluble PEMMCs are formed. If the polyelectrolyte is a weak polyelectrolyte, the process of formation of soluble PEMMCs can be detected by registering changes in the pH of the solution that are produced due to cooperative ionization.<sup>84</sup> After a certain amount of added multivalent molecules, a massive ionic crosslinking takes place, and the system phase-separates. Then, starting with a fixed concentration of polyelectrolyte, when adding increasing amounts of multivalent molecules, the solution transitions from one phase to two phases and then back again into a one-phase solution (Fig. 9a). The critical concentration of multivalent molecules for the system to phase-separate depends on (1) the polyelectrolyte concentration,<sup>118</sup> (2) the ionization degree of the polyelectrolyte<sup>84</sup> (3) the valency of the multivalent molecule,<sup>118</sup> (4) the ionic strength,<sup>119</sup> and (5) the temperature.<sup>120,121</sup> For high enough concentration of multivalent molecules, PEMMCs dissolve completely.<sup>86,122–124</sup> Although this phenomenon is commonly observed for strong polyelectrolytes and many types of multivalent molecules, Delsanti *et al.* demonstrated that mixtures of weak polyelectrolytes like polyacrylate with inorganic multivalent ions like  $\text{Ca}^{2+}$  do not resolubilize at high counterion

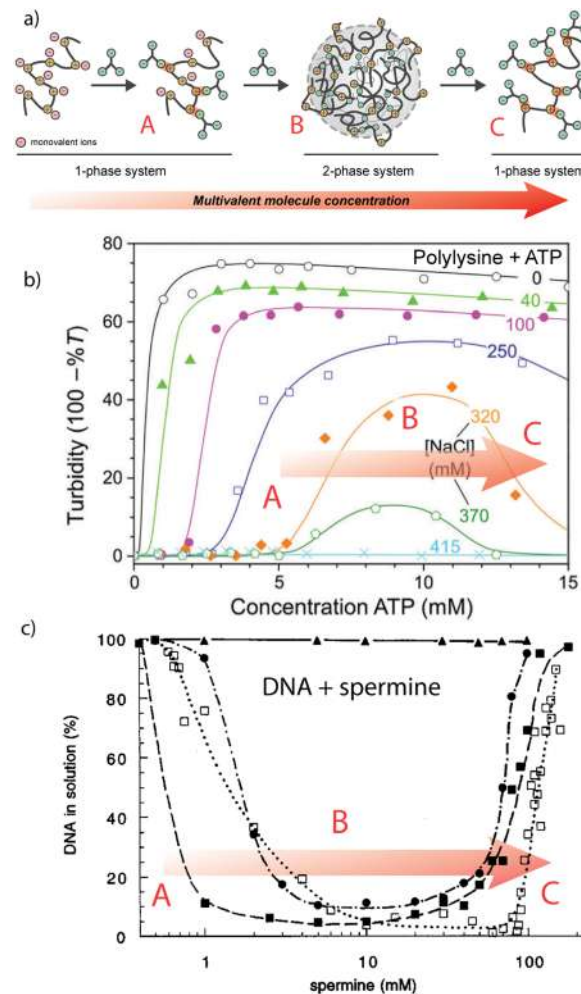


Fig. 9 (a) Schematic representation of the reentrant condensation effect observed in PEMMCs. At low concentration of multivalent molecules (green structures), there is a partial exchange of counterions over the polyelectrolyte chain and the system is a translucent solution (A). At intermediate concentration of multivalent molecules, there is a phase separation (B) driven by the interaction between polyelectrolyte chains and multivalent molecules. For high concentration of multivalent molecules, the system transitions back into a single phase (C). The reentrant condensation effect on PEMMCs can be observed experimentally by measuring the turbidity of the solution at fixed polyelectrolyte concentration and increasing concentration of multivalent molecules. For the system polylysine + ATP ( $z = -3$ ) the turbidity is initially zero, increases at intermediate ATP concentrations, and goes back to zero at high ATP concentration. Figure adapted and reproduced with permission from ref. 111 Copyright (2018) Royal Society of Chemistry. (b). With high enough concentration of monovalent salts, the phase separation is hindered. The same trend can be observed for the system DNA + spermine ( $z = +4$ ) when measuring the percentage of DNA in solution after centrifugation for different mixtures at fixed DNA concentration and variable spermine concentrations. (c). Figure adapted and reproduced with permission from ref. 86 Copyright (1996) American Society for Biochemistry and Molecular Biology.

concentration (before the limit of salt solubility).<sup>125</sup> This effect was attributed to the formation of dehydrated complexes that were unable to resolubilize, and resembles to the case of hydrophobic PECs with salt resistances beyond the limit of monovalent salt solubility.<sup>14</sup> Strictly speaking, we do not consider inorganic multivalent ions as multivalent molecules, however,

both polyelectrolyte-multivalent ion and PEMMC systems are closely related as it will be discussed in next section.

Mechtaeva *et al.* studied the formation of poly(acrylic acid)-based PEMMCs using linear oligoamines with variable charge and chain length from ethylenediamine to pentaethylene-hexamine.<sup>83</sup> Turbidimetry measurements were performed to determine the functional group ratios (NH/COOH) at which PEMMCs were formed. As the multivalent molecule concentration increases, a maximum of turbidity is detected, indicating that there are three phase behavior regions (A, B and C). In region A PEMMCs behaves as partially titrated soluble complexes with no or low turbidity, whereas dispersed solid PEMMCs with a high turbidity appear in region B, and finally, fully titrated soluble complexes with no or low turbidity are present in region C (see scheme in Fig. 9b). Spruijt *et al.* observed the same behavior when studying the system ATP/poly-L-lysine, as turbidimetric plots also showed a maximum turbidity at a given ATP concentration (Fig. 9b).<sup>111</sup> Furthermore, turbidimetric measurements were carried out in the presence of different concentrations of monovalent ions and observed that the critical ATP concentration increased as monovalent salt concentration increased.

Within the framework of polyelectrolyte complex coacervate systems, the reentrant behavior can be explained by looking at the phase diagram depicted in Fig. 5a. Moving from left to right in a horizontal trajectory (constant concentration in the y-axis), the system has two transition points: one corresponding to the entry into the two-phase region and one corresponding to the exit from the two-phase region. Also, increasing the concentration of monovalent ions, the first transition point shifts to the right and the second transition point to the left. For high enough concentration of monovalent ions, the reentrant condensation is suppressed as also seen in PEMMC systems (Fig. 9b). In the next section we will discuss some particularities of the PEMMC phase diagrams and make a comparison with the analogous in PEC systems.

### 3.4. PEMMCs phase diagrams

While the phase behavior of PECs was thoroughly investigated, the aggregation of polyelectrolytes by the addition of multivalent molecules (or short-chain polyelectrolytes) have gained less attention. This is surprising considering that most of PEC features are also present on PEMMC systems. Moreover, due to the versatility of PEMMCs in terms of the free election of the multivalent molecule, these types of complexes can be exploited not only as macroscopic coacervates or layer-by-layer building blocks but also as drug carriers, either by using an electrically-charged drug as a PEMMC component or by adsorption within the complex.<sup>92,126</sup> It is important, therefore, to have a complete picture of the phase behavior of these systems and to make a parallelism with the well-known PECs. Perhaps the most studied system, due to its biological relevance, is the collapse and/or aggregation of DNA chains in the presence of spermine ( $[\text{C}_{10}\text{N}_4\text{H}_{30}]^{4+}$ ).<sup>86,124,127,128</sup> Since DNA is a polyanion and spermine is a multivalent small molecule, the DNA/spermine system can be considered a PEMMC system. First, detailed studies on the phase behavior of DNA in the presence of spermine showed that the system displays a reentrant condensation

behavior (Fig. 9c), and a series of phase diagrams were reported showing that (1) the spermine concentration needed to induce DNA precipitation increases with the concentration of DNA, and (2) the spermine concentration needed to produce the re-solubilization of the aggregate is independent of the DNA concentration (a representative phase diagram of PEMMCs is depicted in Fig. 10a).<sup>124</sup> Moreover, the same characteristic phase diagram was obtained by other authors when studying the phase behavior of synthetic strong and weak polyanions in the presence of inorganic multivalent cations such as  $\text{Ca}^{2+}$  and  $\text{La}^{3+}$ ,<sup>122,125</sup> indicating that the characteristics of the DNA/spermine phase diagram are somehow universal (although we do not consider  $\text{M}^{z+}$  as multivalent molecules, their mixtures with synthetic polyanions behave in the same way as PEMMC

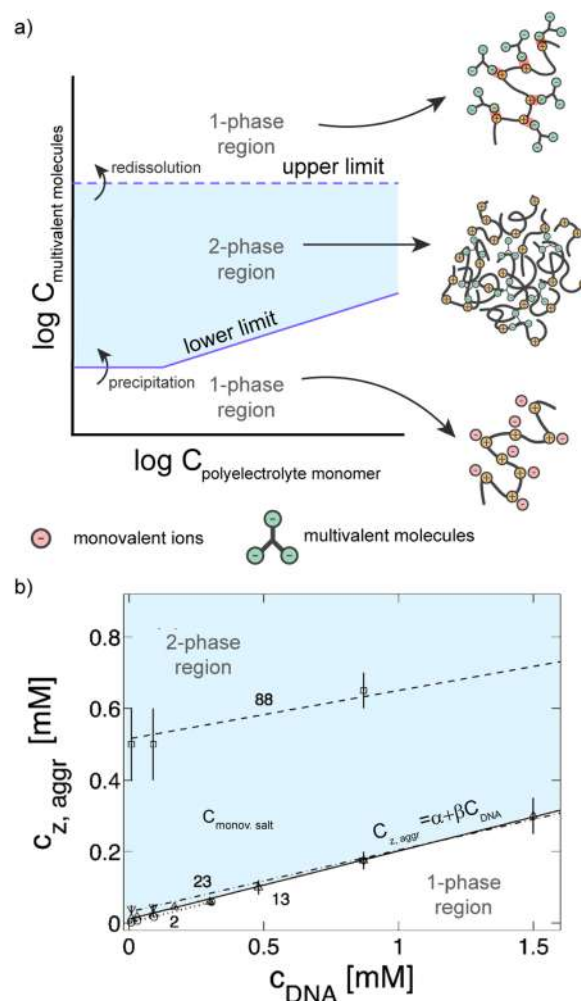


Fig. 10 (a) Schematic representation of the phase diagram of a mixture of a polyelectrolyte and a multivalent ion in aqueous solution at fixed monovalent salt concentration. Usually, the phase diagram is expressed as a log–log plot with the concentration of multivalent ions in the ordinates. Inside the region highlighted in light-blue, the system separates into two phases. While the upper limit was found to be independent of the concentration of polyelectrolyte, the lower region was found to follow a linear dependence as shown in (b). The numbers near to each transition line indicates the concentration of monovalent ions. Adapted and reproduced with permission from ref. 129 Copyright (2003) Cell Press.

systems). Also, it was demonstrated experimentally that the two-phase region tended to disappear at elevated monovalent salt concentration.<sup>122</sup> In a seminal work, Burak *et al.* studied the aggregation of DNA chains in the presence of spermine and demonstrated that the concentration of multivalent molecules in the limit of aggregation ( $c_{z, \text{aggr}}$ ) in fact scale linearly with the concentration of DNA ( $C_{\text{DNA}}$ ) in the form  $c_{z, \text{aggr}} = \alpha C_{\text{DNA}} + \beta$  (Fig. 10b), with  $\alpha$  and  $\beta$  being two parameters related to the density profile of multivalent counterions around isolated DNA chains at the onset of aggregation.<sup>129</sup> The re-solubilization (or chain re-expansion) phenomenon, on the other hand, was tackled by Olvera de la Cruz by means of a thermodynamic two-state model that indicated that the re-solubilization was driven mainly by screening of the electrostatic interactions between polyelectrolyte monomers at elevated multivalent ion concentrations.<sup>130</sup>

PEMCMs and PEC binodal phase diagrams describe similar phenomena, therefore, both phase diagrams should display similar shapes. With this idea in mind, the lower limit curve in Fig. 10a should correspond to the left branch of the PEC phase diagram in Fig. 5a and the upper limit curve in Fig. 10a should correspond to the right branch of the PEC phase diagram in Fig. 5a. Also, according to this hypothesis, the lower and the upper limit curves in Fig. 10a should meet together both as high and low polyelectrolyte concentrations (the phase diagram of a PEMMC system should be closed-loop). Although in some studies the unification of the lower and upper limits at high polyelectrolyte concentrations has been observed,<sup>124</sup> the low polyelectrolyte concentration limit has not been explored yet. A key paper by Zhen-Gang Wang may shed some light on this matter. By using the liquid-state theory, Wang *et al.* constructed a phase diagram for the system polyanion/divalent counterion and showed that the binodal was closed-loop, explaining the reentrant condensation of polyelectrolytes in multivalent salt solutions.<sup>79</sup>

### 3.5. Are PEMCMs chain-length asymmetric PECs?

Although there are no conclusive studies that effectively describe the macroscopic phase separation characteristics of PEMCMs as a special case of PECs in which two polyelectrolytes with a high degree of chain length asymmetry are complexed, most features of PEMCMs were explained computationally in these terms for a reduced number of molecules.<sup>88,110,131–134</sup> In one of these contributions, Zhou *et al.* studied the complex formation between one long polyanion (100 monomers) chain and many short oligocation chains (between 2 to 5 monomers) by Langevin simulations, using a coarse-grained bead-spring model for the polyelectrolyte chains, and small salt ions modeled explicitly.<sup>110</sup> There, Zhou *et al.* found that the polyanion chain collapses into a close-packed globule structure when oligocations are added to the system. The process was found to be driven by the release of monovalent counterions and co-ions. For multivalent molecule concentrations lower than the neutralization point (charge-matching conditions), the globules' charges were negative, indicating that the charge of the cluster is dominated by the long-chain polyelectrolyte. This result is consistent with the

typical features displayed by PEMCMs in which the aggregation occurs in conditions of charge inversion.<sup>128</sup> Above the neutralization point, the charge of the globule becomes positive. With further addition of oligocations, the globule re-expands and its net charge becomes close to zero. The re-expansion of the polyanion chain can be explained in terms of a reduction of the fraction of oligocations that bridge between different chain segments. Interestingly, this behavior was not dependent on the size of the oligocation, meaning that the architecture of the oligocation was not a determining factor. Although this result agrees qualitatively well with PEMCMs systems,<sup>86,122,124,125,127,135</sup> it was demonstrated both computationally and experimentally that the chain flexibility have a profound impact on the characteristic of the complexes obtained from asymmetric polyelectrolytes and PEMCMs.<sup>136,137</sup> Using a different approach, Zhen-Gang Wang studied the effect of chain length asymmetry using dissipative particle dynamics for both single- and multi-chain systems.<sup>88</sup> For a system composed of one polyanion with 200 monomers and one polycation with variable chain-length (ranging from 50 to 200 monomers), the complexes displayed different morphologies depending on the chain-length (Fig. 11a). When using short polycations with less than half of the size of the polyanion, extended overcharged configurations with a tadpole-like morphology were obtained in agreement with experimental observations for the system chitosan/tripolyphosphate.<sup>138</sup> Previously, Zhang *et al.* predicted this type of behavior by theoretical modeling of the complexation process of opposite-charge polyelectrolytes with different chain lengths.<sup>139</sup> For increasing polycation chain-lengths, the clusters condensed into more compact structures. At charge-matching conditions (both polyelectrolytes with equal length), the complexes condensed into globular structures in a similar fashion to Zhou findings. When considering a multi-chain system of 10 polyanion chains with 50 monomers and 10 polycation chains with varying chain-lengths, ranging from 25 to 35 monomers, the simulation predicted that each polycation pairs with one polyanion, forming individual  $1 \times 1$  pairs carrying net negative charges. Macroscopically, this means that for chain-length asymmetric PEC systems in 1:1 molar ratio, all complexes remain soluble. This result indicates that overcharged small PEMCMs are formed before the aggregation point. When the chain length of the polycation reaches a threshold value of 40, larger clusters of several different sizes begin to form, ending with a single large cluster at length-matching conditions (Fig. 11b). Again, this can be considered as the aggregation point in a hypothetical macroscopic system. It is interesting to note that the aggregation point does not coincide with the condition of full titration of charges but to a point in which 80% to 90% of the polyanion charges were neutralized by the “short” polycation.

The effect of monovalent salt ions on this type of system was also studied, although results are somehow non-trivial. In a previous section of this work, it was shown that monovalent salts usually tend to interfere in the PEMMC formation, shifting the point-of-aggregation towards larger concentrations of multivalent molecules (see Fig. 9). In concentration-asymmetric PEC systems, on the other hand, the addition of monovalent salts produces a salting-out phenomenon, which is the inverse effect

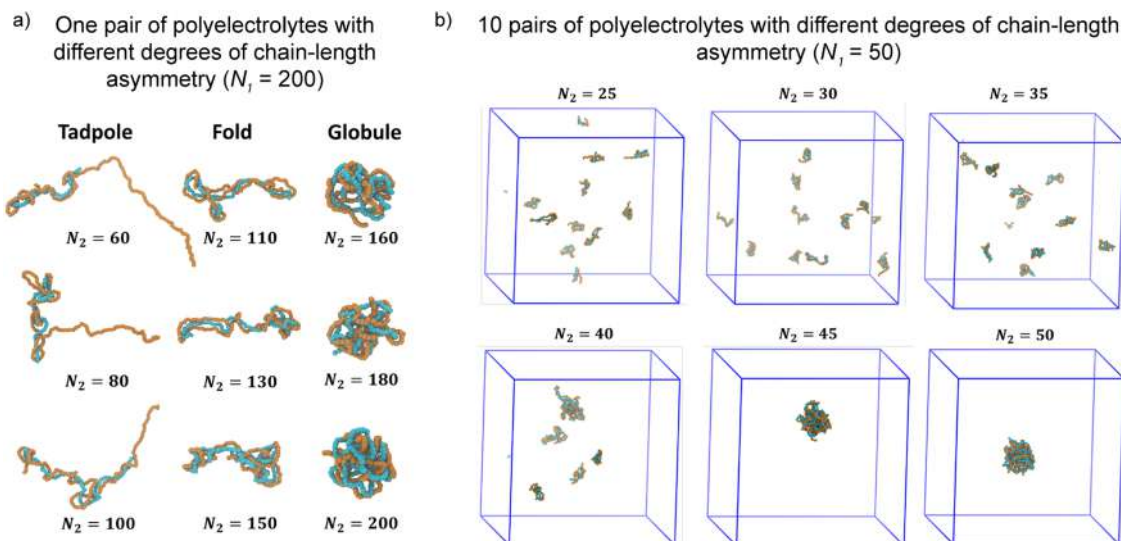


Fig. 11 Structural characteristic of PECs with different degrees of chain-length asymmetry calculated by Wang *et al.* using dissipative particle dynamics. Structures of aggregates formed by interaction of one (a) and ten (b) pairs of oppositely-charged chains with different degrees of asymmetry. The length of the polyanion ( $N_1$ ) is always fixed and the length of the polycation ( $N_2$ ) is varied. Reproduced with permission from ref. 88 Copyright (2022) American Chemical Society.

that occurs in PEMMCs systems (see Fig. 6a, green curve at low total ion concentrations). By studying both charge- and concentration-asymmetry in PEC systems, Zhen-Gang Wang found that monovalent salts produce a salting-out phenomenon followed by a salting-in phenomenon due to electrostatic screening.<sup>77,88</sup> These results are not in agreement with most of PEMMC systems (salting out was not observed for PEMMCs), indicating that it is not enough to study only one type of asymmetry but to study both types of asymmetries and considering bulky systems. At the moment, the similarities and differences between PEMMCs and asymmetric PECs is far from being understood. We believe that the construction of the 2D binodal phase diagrams of PEMMCs and their comparison with the well-known PEC phase diagrams will contribute to the definitive understanding of the system.

## 4. Stimulus-activated PEMMC assembly/disassembly

The phase separation of polyelectrolytes due to complexation with multivalent molecules depends on several factors as (1) the molar ratio, (2) the ionization degree of the polyelectrolyte, (3) the ionic strength, and (4) the valency of the molecule. While the molar ratio is usually fixed, the ionization degree of the polyelectrolyte, the ionic strength, and the valency can be tuned externally by different strategies. When dealing with weak polyelectrolytes, a change in the pH of the solution leads to changes in the ionization degree of the polyelectrolyte. Let us consider a PEMMC system composed of a weak polybase (like a polyamine) and a sufficiently-charged anion at very low pH. In this scenario, the polybase will be fully charged and the system will phase-separate. If a strong base is added to the

solution, the pH can be increased until the polybase is neutral. Under this new condition, all PEMMCs will dissociate completely.<sup>84,118</sup> This process is fully reversible, as the addition of a strong acid will produce the reassociation of species. This is the main principle on why PEMMCs can be either assembled or disassembled simply by changing the pH of the solution. The ionic strength, on the other hand, produces the screening of the electrostatic attraction between species.<sup>95,140</sup> Then, by regulating the ionic strength (adding pure water or adding a monovalent salt), it is also possible to drive the system to assemble or to disassemble.

In Section 3.1, we introduced the concept of valency restriction, that applies over the multivalent molecule in PEMMCs. This means that, for a given polyelectrolyte-multivalent molecule system, there will be a minimum valency required to produce the phase separation (independently of other factors). This minimum valency is normally in the range of  $z = 2$  to  $z = 5$  and depends purely on the chemical structures of the polyelectrolyte and the multivalent molecule.<sup>87</sup> Then, for a system composed of a sufficiently-charge polyelectrolyte and a molecule bearing the minimum valency required to form PEMMCs, a lowering in its valency (no matter how that is achieved) will produce the dissociation of the complex. Conversely, if the multivalent molecule does not have enough charge, an increase in its charge (as that caused by pH changes) can trigger the phase separation.

Temperature has also shown to have an impact on the phase separation phenomenon of PEMMCs.<sup>120,141,142</sup> However, there are no general rules that can be applicable to all PEMMC systems. Depending on the selected building blocks, an increase in the temperature can drive the system either to phase-separation or to dissolution. Generally, the effect of the temperature on the thermodynamics of the system is addressed

in terms of specific non-electrostatic interactions (*e.g.*, base stacking when using nucleotide-base components), that are present within the complexes and that are temperature-sensitive.<sup>120,142</sup>

As most PEMMC building blocks are weak polyions with pH-tunable charge, one of the most explored stimuli to modulate assembly/disassembly is changes in pH. For example, let us consider the pH-response of a colloidal dispersion of poly(allylamine)/phosphate PEMMCs at different ionic strengths.<sup>84</sup> Since phosphate has three acid constants, a decrease in pH results in a decrease in its charge due to partial protonation, which discourages PEMMC formation. On the other hand, alkaline pH also destabilizes the assembly by deprotonation of amines in poly(allylamine). Thus, in the absence of salt, the system can be assembled in a range of pH between 5.7 and 9.7. When 0.2 KCl is added, a much narrower range was observed (6.8 to 8.6) due to the screening effect caused by the high salt concentration that weakens the poly(allylamine)-phosphate interactions. The reduction in the PEMMC pH-stability window by increasing the concentration of monovalent ions can be rationalized in terms of the non-stoichiometric phase diagram of PECs depicted in Fig. 5: an increase in the concentration of monovalent ions produces a shrinking of the two-phase region, therefore, the threshold concentration of multivalent molecules will become closer to the charge-matching conditions. In the case of the poly(allylamine)-phosphate system, this will lead to a shrinking in the range of pH at which the system will phase-separate. Interestingly, the formation/dissolution process with changes in pH was fully reversible.<sup>84</sup> In a similar way, Moya *et al.* studied the effect of pH changes of poly(allylamine)-based PEMMCs using phosphate-based molecules with different lengths.<sup>143</sup> They observed that the pH range in which PEMMCs are formed widens according to the increment in the number of phosphate groups per molecule.

In another recent approach, hexacyanoferrate anions ( $[\text{Fe}(\text{CN})_6]^{3-}$  and  $[\text{Fe}(\text{CN})_6]^{4-}$ ) were combined with polyethylenimine in aqueous solution to form PEMMC nanocomplexes with responsiveness to multiple stimuli (Fig. 12d).<sup>118</sup> In order to clearly understand the response of this system, a series of phase diagrams were constructed at fixed monovalent salt concentration. Fig. 12 shows three phase diagrams in three different conditions: pH = 3.5 without added monovalent salt (Fig. 12a), pH = 3.5 with 0.2 M NaCl (Fig. 12b), and pH = 9 without added monovalent salt (Fig. 12c). Each of the three plots is an overlay of two phase diagrams: one for polyethylenimine/ $[\text{Fe}(\text{CN})_6]^{3-}$ , and one for polyethylenimine/ $[\text{Fe}(\text{CN})_6]^{4-}$ . All of these phase diagrams show only a small region of the entire phase diagram (like the one depicted in Fig. 5a). It is important to note that the line that separates the one-phase and the two-phase regions corresponds to a non-stoichiometric condition with an excess of anions. Note also that phase diagrams at pH = 3.5 have a narrow region in which PEMMCs are thermodynamically stable only for the system polyethylenimine/ $[\text{Fe}(\text{CN})_6]^{4-}$ . This means that, in this region, the system is redox-sensitive. In fact, it was demonstrated that starting with polyethylenimine/ $[\text{Fe}(\text{CN})_6]^{4-}$ , the addition of  $\text{KMnO}_4$  produced the dissolution of PEMMCs by

oxidation of  $[\text{Fe}(\text{CN})_6]^{4-}$  to  $[\text{Fe}(\text{CN})_6]^{3-}$  (valency reduction). On the other hand, starting with polyethylenimine/ $[\text{Fe}(\text{CN})_6]^{3-}$ , the addition of ascorbic acid produced the formation of PEMMCs by reduction of  $[\text{Fe}(\text{CN})_6]^{3-}$  to  $[\text{Fe}(\text{CN})_6]^{4-}$  (valency increment). When comparing the phase diagrams without added monovalent salt at pH = 3.5 and pH = 9, it can be observed that the slopes of the transition curves increase at alkaline pH. This is trivial since as polyethylenimine is titrated by  $\text{OH}^-$ , loses its charge, therefore, less multivalent molecules are needed to produce the phase separation. In addition, excess  $\text{OH}^-$  eventually hinders the formation of PEMMCs, independently of the concentration of the other species. The change in the slope can be further exploited to drive the system either to assembly or to disassembly by altering the pH of the solution. Finally, the addition of NaCl produces a shift in the transition curve of the  $[\text{Fe}(\text{CN})_6]^{3-}$  phase diagram, thus making the polyethylenimine/ $[\text{Fe}(\text{CN})_6]^{3-}$  system sensitive to changes in the ionic strength. Spruijt *et al.* reached similar conclusions when working with the system  $[\text{Fe}(\text{CN})_6]^{3-}$  (or  $[\text{Fe}(\text{CN})_6]^{4-}$ )/poly-L-lysine as they observed that, in the presence of a moderated concentration of monovalent ions, there is a region in which the system phase separates only with  $[\text{Fe}(\text{CN})_6]^{4-}$ .<sup>112</sup> Then, if an oxidizing agent like  $\text{S}_2\text{O}_8^{2-}$  is added, the iron complex oxidizes to  $[\text{Fe}(\text{CN})_6]^{3-}$  and the solution gets yellowish transparent (coacervate droplets dissolve completely). Furthermore, the process was shown to be reversible, as the addition of glutathione (GSH) or NADH produced the reduction of  $[\text{Fe}(\text{CN})_6]^{3-}$  to  $[\text{Fe}(\text{CN})_6]^{4-}$  and PEMMC coacervate droplets formed again (Fig. 12e).

Recently, a photo-, redox-, and thermo-responsive PEMMC based on branched polyethylenimine and the trianionic complex ferrioxalate was reported.<sup>121</sup> When ferrioxalate is irradiated with UV-light, or a reducing agent is added to the system, the trianionic complex decomposes (or reduces) to a dianionic complex that is no longer able to efficiently act as ionic cross-linker (Fig. 12f and g). Thus, the stimuli-induced reduction of the valency produces the disassembly of the PEMMC. Additionally, the system showed that the assembly/disassembly process can also be modulated by changing the temperature of the environment. The increase in temperature activates the PEMMC disassembly, until reaching a completely translucent solution above 35 °C (Fig. 12h). When cooled down to 5 °C, the PEMMC nanocomplex configuration was recovered, confirming the reversible behavior of the system in response to temperature changes. The temperature response was explained in terms of a variation in the association constant of polyethylenimine and ferrioxalate with the temperature (the process of PEMMC formation in this case was exothermic). A temperature-dependent reversible behavior was also observed for coacervates based on polypeptides (poly-L-lysine, poly-L-arginine and protamines) complexed with multivalent anions (nucleoside triphosphate, tripolyphosphate and citrate).<sup>120,144</sup>

Enzymes can also be used as biorelevant stimuli to modulate the formation and disassembly processes of PEMMCs. As an example, Huang *et al.* reported a phosphatase-responsive system composed of chitosan and adenosine-5'-triphosphate (ATP) as an enzyme-sensitive multivalent molecule. In the presence of the active phosphatase, ATP ( $z = -3$ ) can be hydrolyzed to single

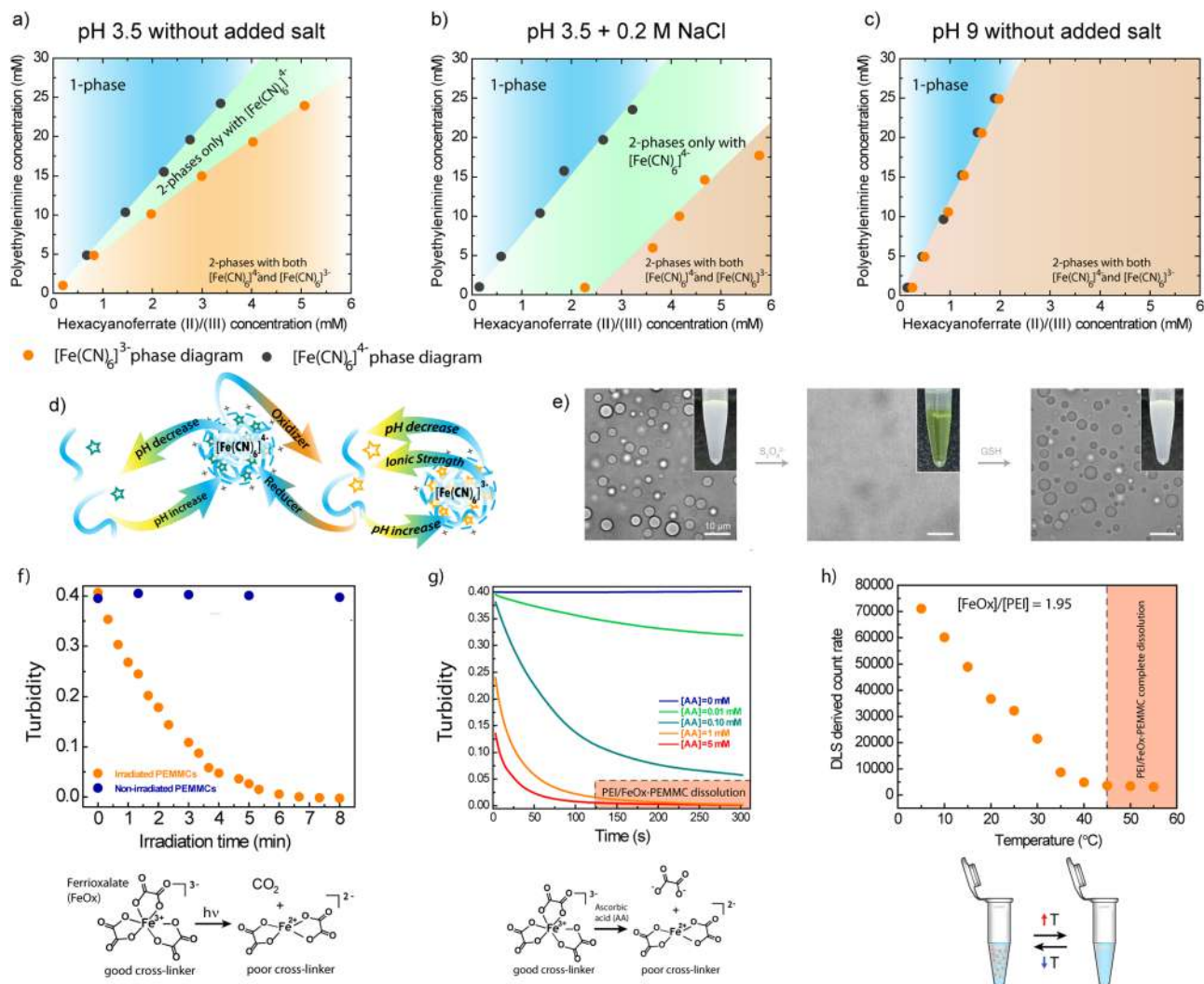


**Fig. 12** (a–c) Overlaid non-stoichiometric phase diagrams of polyethyleneimine-based  $[\text{Fe}(\text{CN})_6]^{4-}$ -PEMMCs (grey dots) and  $[\text{Fe}(\text{CN})_6]^{3-}$ -PEMMCs (orange dots) at different conditions: pH 3.5 without added salt (a), pH 3.5 plus 0.2 M NaCl (b), and pH 9 without added salt (c). Inside the one-phase region (light blue), no PEMMCs are formed. Inside the two-phase region (green), PEMMCs are formed only when  $[\text{Fe}(\text{CN})_6]^{4-}$  is used. In the orange region, PEMMCs are formed with both  $[\text{Fe}(\text{CN})_6]^{4-}$  and  $[\text{Fe}(\text{CN})_6]^{3-}$ . These phase diagrams can be exploited to assemble or to disassemble PEMMCs using different stimuli such as pH, ionic strength, and changes in the redox state of the Fe complexes (d). Reproduced with permission from ref. 118. Copyright [2020] Royal Society of Chemistry. (e) Optical microscope images of dissolution of  $[\text{Fe}(\text{CN})_6]^{4-}$ /poly-L-lysine coacervate droplets by  $\text{S}_2\text{O}_8^{2-}$  addition and the formation of coacervate droplets by GSH addition. The insets show photographs of the corresponding turbid suspensions or the clear solution. (f–h) Photo-, redox-, and thermo-responsive polyethyleneimine/ferrioxalate PEMMC: (f) photoactivated dissolution of PEMMCs by decomposition of ferrioxalate (valency reduction); (g) PEMMC dissolution by the addition of different concentrations of ascorbic acid (AA) (valency reduction) and (h) PEMMC (reversible) dissolution by increasing the temperature from 5 to 55 °C (the y-axis measures the turbidity of the solution in terms of the dynamic light scattering derived count rate). Reproduced with permission from ref. 121 Copyright [2019] Royal Society of Chemistry.

phosphates ( $z = -2$ ) and neutral adenosine causing the enzyme-mediated disassembly of the aggregates.<sup>145</sup> Keating *et al.* studied the ability of the enzyme phosphatase to activate the formation of coacervates in mixtures of anionic RNA and a oligopeptide with phosphorylatable serines.<sup>146</sup> Enzymatic dephosphorylation increases the cationic charge of the oligopeptide, activating the formation of coacervates. Interestingly, this process can be reversed by applying a kinase A enzyme to re-phosphorylate the oligopeptide and remove its cross-linking ability. As we will see later, the study of the enzymatic reactions on organized supramolecular compartments such as PEMMCs is extremely

important to explore biorelevant processes under simulated conditions.

## 5. Applications

The diverse and interesting characteristics of PEMMCs (including an easy, sustainable and supramolecular preparation route; an extensive and varied library of potential building blocks; the ability to adopt different architectures such as nanocomplexes and coacervates, and an assembly/disassembly process easily

modulated with specific stimuli) triggered the study of these materials in a wide range of technological fields. For instance, PEMMCs were evaluated as smart nanocarriers of bioactive molecules, precursors of functional films and adhesives, and mimics of protocells and membraneless organelles.<sup>30,147,148</sup> Next, we will examine the most relevant developments in the set of applications described.

### 5.1. Drug delivery

PEMMCs, in both nanoparticle and coacervate configuration, have a great capacity to load different bioactive molecules, including antitumor and antimicrobial drugs, imaging agents, genes, enzymes, and food additives, making these materials promising candidates for controlled delivery.<sup>30,31,40,148,149</sup> In general, two strategies have been exploited to encapsulate cargo into PEMMCs: the incubation method and the incorporation method.<sup>37</sup> In the incubation method, a given amount of cargo is added to the solution containing pre-formed PEMMCs (post-synthesis method). In the incorporation method, the cargo addition is made out before the complexation process (pre-synthesis method). After encapsulation, loaded PEMMCs are separated by centrifugation. Another attractive strategy is to use the bioactive molecule itself as a PEMMC building block, which guarantees very high encapsulation efficiencies.<sup>126,150</sup> This can be done only if the bioactive molecule possesses enough charge as discussed in previous sections of this work.<sup>30,151,152</sup> In addition to the efficient sequestration of the cargo molecule, PEMMCs offer protection for the agent when it is exposed to certain environmental conditions such as extreme temperature, light, and pH, among others.<sup>40,153,154</sup> On the other hand, as discussed in the Section 4, these platforms are able to respond to the presence of specific stimuli that alter the charge of their building blocks causing the matrix disassembly and the selective cargo release. With the advent of stimuli-responsive materials, the scientific community came up with powerful approaches for the precise and controlled release of bioactive molecules.<sup>155–157</sup> In this sense, by exploiting the presence of a specific stimulus, drug delivery can avoid non-specific tissue interactions and minimize drug side effects. With this aim, different internal stimuli such as pH gradients, redox potentials, and overexpressed metabolites and enzymes can be considered. At the same time, external stimuli such as light irradiation, temperature, ultrasound waves, and electromagnetic fields can also be exploited.

**5.1.1. PEMMC nanocomplexes.** Taking advantage of the pH-sensitivity of the phosphate anion, Moya and co-workers encapsulated silencing RNA (siRNA) into poly(allylamine)/phosphate PEMMC nanocomplexes and, by *in vitro* studies, evaluated their capacity as pH-sensitive nanocarriers for the intracellular delivery of genetic materials.<sup>158</sup> After cellular internalization by endocytosis, PEMMCs disassemble due to the low endosomal pH, triggering the release of siRNAs into the cytoplasm. The result obtained confirms that poly(allylamine)/phosphate complexes have the potential to act as smart nanocarriers in gene therapies. The pH-sensitivity of PEMMCs was also explored to design systems responsive to glucose gradients present in

metabolic diseases such as diabetes.<sup>159–161</sup> To achieve a selective response, a glucose-responsive material is incorporated into the delivery platform, such as the glucose oxidase enzyme (GOx).<sup>162,163</sup> GOx catalyzes the oxidation of D-glucose to gluconic acid, which, in turn, reduces the local pH. Considering the above, a four-component glucose-responsive poly(allylamine)/phosphate PEMMC system containing GOx and insulin was designed achieving supramolecular particles with a typical hydrodynamic diameter of 350 nm (see scheme in Fig. 13a).<sup>164</sup> Under hyperglycemic conditions (10, 15 and 20 mM glucose), an acidic environment is produced, which leads to the protonation of phosphates (valency reduction) and activates the PEMMCs disassembly. As a consequence, all insulin peptides are released whenever glucose overcomes a threshold concentration (Fig. 13b). In a similar approach, Anderson *et al.* used the electrospray technique to fabricate glucose-sensitive chitosan/tripolyphosphate PEMMCs, although in this case, the release of insulin was achieved by swelling of the complexes due to electrostatic repulsion between the polymeric chains generated by the protonation of the amine groups of chitosan under hyperglycemic conditions.<sup>162</sup>

The overexpression of certain enzymes in specific environments can be exploited to generate intelligent PEMMCs.<sup>165–169</sup> Gupta and coworkers exploited the susceptibility of poly-L-lysine to biodegradation by proteolytic enzymes to build protease-responsive PEMMCs (Fig. 13c).<sup>170</sup> A nanosystem for specific delivery of contrast agents was designed by encapsulating the fluorescent dye indocyanine green in aggregates of poly-L-lysine assembled with a mixture of phosphates and citrate anions. These authors showed that PEMMC nanocomplexes can be absorbed by the cells through endocytosis and degraded in the presence of a proteolytic enzyme in the lysosomal compartments, activating the selective release of indocyanine green and producing the specific imaging of cells (Fig. 13d).

Recently, a dual and sequential pH/enzyme response system by assembling biodegradable poly-L-lysine dendrigraft with tripolyphosphate was reported (Fig. 13e).<sup>171</sup> The complexing of peptide dendrimers (~7 nm in diameter) leads to the formation of supraparticles with defined size (~200 nm-diameter) that are stable at physiological pH. At mildly acidic pH, the supraparticles are disassembled, activating a first-stage size transition in accordance with the restitution of the free dendrimer. Carrier size changes triggered by internal stimuli are sought after in antitumor therapies to overcome the size paradox of anticancer nanopharmaceuticals. This paradox is related to the fact that nanocarriers with a size of about 100–200 nm show good tumor accumulation but have limited tissue penetration ability. In contrast, particles smaller than 10 nm are capable of penetrating deep into the tumor, but at the same time are rapidly cleared by the systemic circulation. Going back to the dendrigraft/tripolyphosphate system, a molecule cargo can remain efficiently encapsulated in the dendritic architecture after the PEMMC size-reduction from 200 to 7 nm. Subsequently, cargo release can be triggered in a second stage by the action of the enzyme trypsin (overexpressed in tumor cells) through biodegradation of the peptide dendrimer (Fig. 13e). Interestingly,

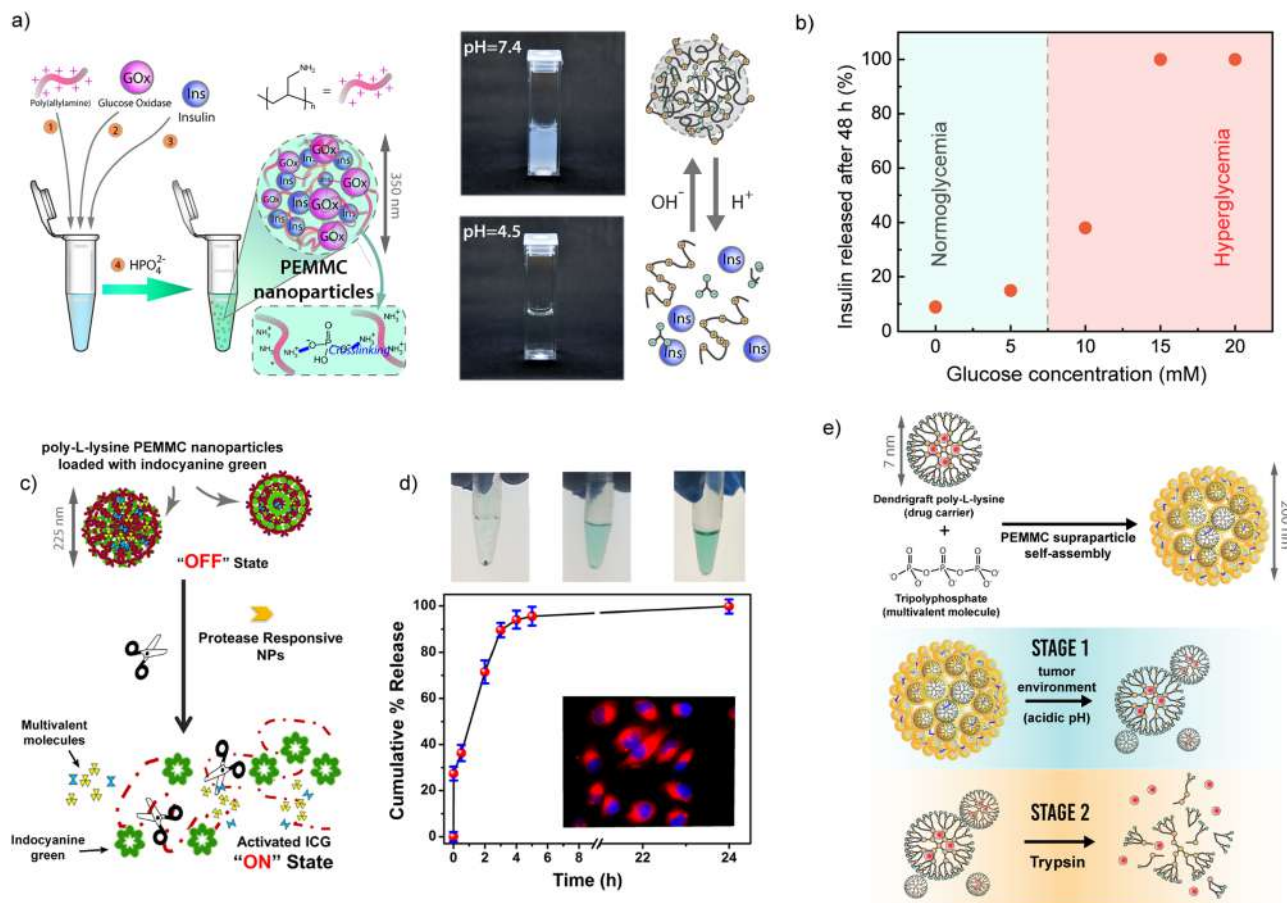


Fig. 13 Stimuli-responsive PEMMCs nanocomplexes for drug delivery. (a) Formation of insulin-containing glucose-responsive poly(allylamine)/phosphate PEMMCs and their pH-activated assembly/disassembly by altering the charge of the phosphate ion; (b) insulin release profile at different concentrations of glucose (Adapted and reproduced from ref. 164 Copyright [2019] Wiley-VCH Verlag GmbH & Co.); (c and d) enzyme-responsive poly-L-lysine/phosphate-citrate PEMMCs and indocyanine green cumulative release. Inset shows the activation of cell imaging by indocyanine green releasing after PEMMC endocytosis. Adapted and reproduced with permission from ref. 170 Copyright [2019] Nature Springer; (e) self-assembly of poly-L-lysine dendrigraft with tripolyphosphate and sequential pH- and enzyme responsiveness for multistage drug delivery. Adapted and reproduced with permission from ref. 171 Copyright [2020] Elsevier.

supraparticles exhibited great capacity to encapsulate molecules of variable charge, including therapeutic drugs, such as doxorubicin and curcumin. We believe that the proposed strategy has potential in the application of multistage drug delivery systems for promoting both deep tissue penetration and spatiotemporal controlled drug delivery.

Light and temperature have also been applied as external stimuli for controlled release.<sup>172–176</sup> For achieving this goal, building blocks are typically functionalized with groups sensitive to a specific stimulus.<sup>177–182</sup> For example, chitosan was grafted with the thermo-sensitive polymer poly(*N*-vinylcaprolactam), and complexed with tripolyphosphate.<sup>183</sup> The complexes increase in size with increasing temperature in the phase transition range of the copolymer (39–45 °C). The size increase is due to the aggregation of the particles by hydrophobic interactions enhanced by heating. The nanocomplexes showed a temperature-dependent release rate of doxorubicin (DOX), possibly due to changes in the drug/nanocomplex affinity caused by heating, altering the DOX partition equilibrium and promoting its release. In another similar approach, chitosan was functionalized with the

chemotherapeutic agent 5-fluorouracil using a linker susceptible to photocleavage under 365 nm UV-A irradiation.<sup>184</sup> By complexation of the conjugated polymer with tripolyphosphate, a suspension of PEMMC nanocomplexes was obtained on which the releasing of 5-fluorouracil was controlled by the light dose applied.

**5.1.2. PEMMC coacervates.** Coacervate PEMMCs were less explored as delivery platforms compared to nanocomplexes. This may be surprising considering the vast library of works on microencapsulation mediated by conventional coacervation between two oppositely charged macromolecules.<sup>149,185–188</sup> Lapitsky *et al.* evaluated the delivery properties of PEMMC coacervates based on poly(allylamine) and multivalent phosphates (tripolyphosphate and pyrophosphate). First, they used two model small molecules as cargo molecules: anionic Green FCF and zwitterionic Rhodamine B dyes.<sup>189</sup> They found that the system efficiently encapsulated both payloads and that they can be released over a time-scale of several months. Subsequently, the same authors encapsulated the weakly amphiphilic anion ibuprofen in poly(allylamine)/tripolyphosphate coacervates.<sup>190</sup>

The interaction between the drug and poly(allylamine) leads to extremely high drug loading capacities, with ibuprofen comprising up to about 30% of the mass of the coacervate. The presence of tripolyphosphate weakens the interaction between the drug and the polymer, but at the same time it forms a dense crosslinking matrix, resulting in very slow-release rates, where the diffusion of ibuprofen can extend for periods greater than 6 months (Fig. 14b). Interestingly, when the authors replaced ibuprofen with strong anionic amphiphiles, such as sodium dodecyl sulfate and sodium dodecylbenzenesulfonate, the stronger amphiphile/polyelectrolyte binding disrupts the association between poly(allylamine) and tripolyphosphate. This increased the permeability of the matrix to small molecules, significantly decreasing the time scale (days) of diffusion through the poly(allylamine)/tripolyphosphate network. Thus, the addition of strong amphiphilic structures can be used to modulate the encapsulation and release properties of coacervates.

In other reports, the ability of coacervates to encapsulate and controllably release biocidal agents has been studied.<sup>191,192</sup> In one of these contributions, triclosan was used as a model hydrophobic bactericide. By dispersing triclosan in a poly(allylamine) solution containing non-ionic surfactants, the biocide was efficiently encapsulated after the addition of

tripolyphosphate. Once encapsulated, the active agent exhibits extended-release kinetics of several months that can be easily modulated by varying the bactericide and surfactant compositions (Fig. 14c). The controlled release gives the coacervates sustained bactericidal activity against model Gram-positive and Gram-negative bacteria (*Staphylococcus aureus* and *Escherichia coli*) for at least two weeks. Recently, this study was extended using cetylpyridinium chloride as a model cationic amphiphile. Here, the authors observed that coacervates can also load a cationic surfactant efficiently (with loading capacities exceeding 20 wt%) and release it over multiple-month timescales (Fig. 14d).

## 5.2. Functional coatings and films

Polyelectrolytes have been widely exploited as building blocks of functional films by the layer-by-layer (LbL) assembly technique.<sup>193,194</sup> Since its appearance, this powerful technique allowed to combine different oppositely-charged building blocks to build films and coatings with a wide spectrum of applications in biomedicine, sensing, energy, advanced materials, among others.<sup>195</sup> Typically, in the LbL technique, charged macromolecules are first adsorbed over pre-treated surfaces. Then, alternating layers of oppositely-charged polyelectrolytes are adsorbed to create a film containing a mixture of polyelectrolytes.<sup>196,197</sup> Although the surface-templated adsorption of oppositely-charged polyelectrolytes has been treated differently with respect to PECs formed in solution, Debais and Tagliacucchi recently proposed that both PEC and LbL formation phenomena can be described within the same theoretical formalism, and theoretically confirmed a previously proposed relationship between the salt resistance in PEC phase diagrams and the optimal salt concentration for LbL deposition.<sup>198,199</sup> As it was introduced in Section 3, under non-stoichiometric conditions, PEMMC nanocomplexes display a net charge on their surface. On the other hand, PEMMC nanocomplexes tend to interact strongly with oppositely-charged macromolecules, therefore, they are good candidates to be used as LbL building blocks. Recently, bromophenol blue-loaded poly(allylamine)/phosphate nanocomplexes with a typical hydrodynamic diameter of 100 nm and a  $\zeta$ -potential of 30 mV have been used as cationic building blocks for the preparation of (PEMMC(+)/polystyrene sulfonate(-))<sub>n</sub> LbL thin films, where *n* represents the number of deposited layers.<sup>200</sup> The films showed a linear growth within 10 deposition cycles and thicknesses that were 5 times higher than the standard polycation/polyanion LbL films (Fig. 15a). In addition, the release rate of the bromophenol blue was tuned by exposing the film to different aqueous solutions. When the film was soaked in phosphate-buffered saline solution at pH = 7.4, 80% of the dye was released over a period of 100 hs. In the presence of slightly acidic or alkaline media, the same amount of dye was released in a 24 h window. When exposing the film to more extreme pHs, the dye was released in a few hours.<sup>200</sup> In a similar approach, Muzzio *et al.* fabricated antibacterial multilayer films combining poly-L-lysine and PEMMC nanocomplexes based on poly(acrylic acid) and the antibiotic gentamicin (*z* = +5) (Fig. 15b).<sup>126</sup> Films presented an initial burst release of 58% of the total gentamicin in the first

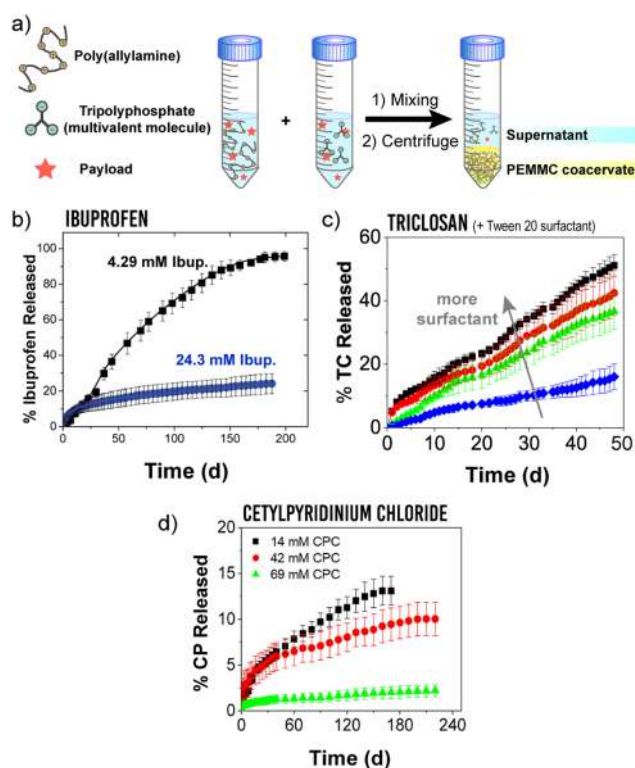
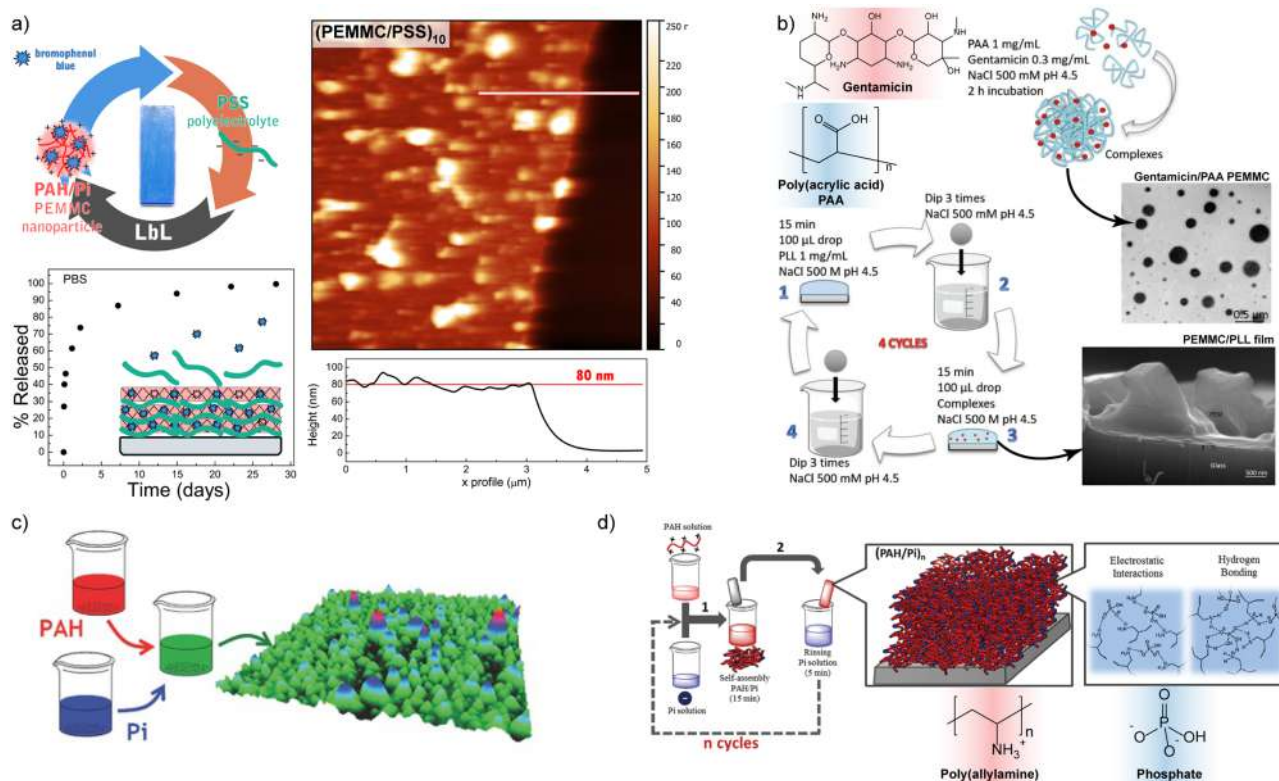


Fig. 14 (a) Simplified representation of the preparation process of drug-loaded PEMMC coacervates composed of poly(allylamine) and tripolyphosphate. Release kinetics of (b) ibuprofen. Reproduced with permission of ref. 190 Copyright [2018] Royal Society of Chemistry; (c) triclosan with various concentrations of Tween 20 surfactant. Adapted and reproduced with permission of ref. 191 Copyright (2020) American Chemical Society; and (d) cetylpyridinium chloride. Reproduced with permission of ref. 192 Copyright (2021) Elsevier.



**Fig. 15** PEMMCs-based films and coating. (a) layer-by-layer assembly of bromophenol blue-loaded poly(allylamine)/phosphate PEMMCs and polystyrene sulfonate, AFM topography images and estimated thickness for 10 cycles of deposition, and dye release over time. Adapted and reproduced with permission from ref. 200 Copyright (2019) Wiley-VCH Verlag GmbH & Co. (b) Formation of PEMMC nanocomplexes based on poly(acrylic acid)/gentamicin (transmission electron microscopy image of nanocomplexes), assembly of antibacterial multilayer films of poly-L-lysine/PEMMC nanocomplexes and SEM cross-sectional image of the films. Adapted and reproduced with permission from ref. 126 Copyright (2019) Wiley-VCH Verlag GmbH & Co. (c) surface-coating based on the self-assembly of poly(allylamine)/phosphate PEMMCs. Adapted and reproduced with permission from ref. 210 Copyright (2015) Wiley-VCH Verlag GmbH & Co., and (d) continuous assembly of poly(allylamine)/phosphate PEMMCs through multiple deposition steps. Adapted and reproduced with permission from ref. 211 Copyright (2019) Royal Society of Chemistry.

6 h, followed by a sustainable release over several weeks. Furthermore, films were effective in preventing the proliferation of the *Staphylococcus aureus* bacteria.

Although the LbL approach has attractive properties as a coating technique,<sup>201–203</sup> its industrial scaling and commercial application remains a considerable challenge as its multiple preparation steps are time-consuming and labor-intensive.<sup>204</sup> In this scenario, simpler strategies have been explored that, while preserving the advantages of the LbL assembly, allow overcoming some of its disadvantages.<sup>205</sup> The direct one-pot deposition of pre-formed PECs in aqueous solution<sup>206</sup> is an attractive approach to generate thin films in a single step.<sup>204</sup> Although the first studies focused on the formation of functional films using two-polyelectrolytes complexes as precursors,<sup>207–209</sup> in recent years, PEMMC components have been exploited too. Azzaroni and co-workers have developed a powerful and versatile substrate-independent self-assembly strategy for poly(allylamine)/phosphate aggregates that allows generating nanofilms by simply immersing the substrate in an aqueous solution containing PEMMCs (Fig. 15c).<sup>210</sup> Here, the concentrations of the polyelectrolyte and the multivalent molecule are tuned to generate a dispersion of PEMMC coacervate droplets that tend to adsorb and

coalesce over the substrate. The authors demonstrated that this approach leads to the formation of thin films of easily adjustable thickness by varying the concentrations of the precursors or the deposition time. Interestingly, these films showed attractive properties for electroless metallization and cell adhesion. In addition, the functionalization of the polymer with different active molecules allowed to easily obtain redox-active surfaces and architectures for biorecognition. Very recently, it was shown that it is possible to successively assemble poly(allylamine)/phosphate PEMMCs through multiple deposition steps, easily modulating the thickness of the coatings and the amount of material deposited (Fig. 15d).<sup>211</sup>

As described in the preceding paragraphs, PEMMCs have generally been used as building blocks of thin coatings. Few reports can be found where the PEMMCs are exploited to produce free-standing films.<sup>212</sup> At this point, there is an important gap compared to PECs that, taking advantage of the plasticizing properties mediated by water and salt, have been exploited to build surface materials. Schlenoff and co-workers were the first to process PDDA/PSS PECs by different strategies (including ultracentrifugation, extrusion and spin coating) to obtain functional solid films.<sup>13,213,214</sup> Recently, Kurtz *et al.*, fabricated bacterial

antifouling films prepared from spin-coating of PDDA/PSS PECs.<sup>204</sup> In other approaches, Mano and collaborators used CS/alginate and CS/chondroitin sulfate PECs to fabricate membranes for tissue engineering applying the solvent casting technique.<sup>215,216</sup> This background indicates that attractive opportunities exist to explore single polyelectrolyte complexes in the construction of functional substrate-free films.

### 5.3. Applications of biomimetic coacervates

After their discovery, over time coacervates acquired great relevance from a biological perspective since processes similar to coacervation appear in cellular membranes and compartments in both prokaryotic and eukaryotic organisms.<sup>54</sup> In this sense, different authors have postulated that the complex coacervation could have played a relevant role in the origin of life.<sup>217</sup> Bungenberg de Jong *et al.* postulated the presence of coacervate-like aggregates in bacterial nucleoid and prokaryotic cell membranes.<sup>2</sup> In addition, similarities with the characteristic coacervate complexes have been found in compartmentalized fluids present in eukaryotic cells such as germ-line P granules, stress granules, nucleoli, and protein/RNA droplets.<sup>54,218,219</sup> More recently, the formation of complex coacervates has been found to be an extremely important process in marine organisms such as mussels, squid, and sandcastle worms.<sup>220–222</sup> These species produce coacervates based on a cocktail of polyelectrolytes that act as underwater adhesives that, thanks to their low surface tension in water, can wet, coat or infiltrate target surfaces and environments.<sup>50,51,223</sup>

In recent decades, the presence of coacervate complexes in living organisms served as an inspiration for the development of biomimetic materials to understand and mimic cellular processes on the one hand, and for the design of underwater adhesive on the other. Below we will discuss the main advances in these fields for PEMMCs coacervates.

**5.3.1. Underwater adhesives.** The deep knowledge about the underwater adhesion mechanisms developed by marine organisms, such as the sandcastle worm and mussels, served as inspiration for the design of a large library of materials with great potential in biomedical, domestic and industrial applications.<sup>224,225</sup> The adhesion mechanisms of marine animals in wet environments finely combine weak interactions, catechol chemistry, and polyelectrolyte complexation.<sup>226–229</sup> Due to the similarity with biofabricated materials, polyelectrolytes have been exploited as building blocks in biomimetic adhesion strategies.<sup>230–232</sup>

In general, polyelectrolytes were combined with catechol groups to generate complex coacervates with strong adhesive properties.<sup>229,233</sup> However, the synthesis of polymers with catechol groups involves complex and expensive processes. Some reports have integrated catechol moiety-containing polyphenols with polyelectrolytes to generate coacervate-based glues by simpler ways.<sup>234,235</sup> In a recent report, the natural polyphenol tannic acid was assembled by ionic interactions and hydrogen bonds with the polycation polyamidoamine-epichlorohydrin to generate underwater adhesive through a direct and sustainable engineering route (Fig. 16a).<sup>236</sup> In addition to the great adhesion capacity on various

surfaces, the material presented bactericidal capacity due to the synergistic combination of the intrinsic antibacterial activity of both the polyphenol and the polycation.

Despite the attractive properties of catechol-based glues, their long-term efficiencies may be affected due to autoxidation of catechol functions. In this context, adhesives based on catechol-free coacervates have been proposed, including PEMMCs coacervates.<sup>148,226,237–239</sup> Lapitsky and co-workers evaluated coacervates of poly(allylamine) complexed with pyrophosphate or tripolyphosphate as underwater adhesives (Fig. 16b).<sup>119,240</sup> Both PEMMC coacervates were shown to be highly rigid, self-healing, and strongly adhesive in aqueous environments on hydrophobic (*e.g.*, skin and Teflon) and hydrophilic (*e.g.*, glass) substrates. Interestingly, these materials showed modulable adhesive properties with changes in pH and ionic strength. From rheological studies, the authors found that adhered coacervates exhibit greater stability at near-neutral or slightly alkaline pH values (of roughly 6.5–9) and at low ionic strengths. Outside the pH range of stability or at high ionic strength, the stability and adhesion of the material decreases considerably due to decreased stability of the PEMMC (ion pairs are disrupted). Interestingly, this responsiveness to changes in pH and ionic strength can be rationally exploited to form or dissolve adhesives on demand.

Very recently, different polycations, such as poly(diallyldimethylammonium), polyethylenimine, poly(allylamine), and quaternized chitosan, were complexed with a  $\pi$ - $\pi$  stacked folic acid quartet to obtain coacervates that were able to interact with a wide variety of substrates *via* polyvalent hydrogen bonding, coordination, and electrostatic interactions (Fig. 16c).<sup>241</sup> After preparation, the water was evaporated and the coacervate was molded into a flexible non-adhesive film, which recovers its adhesive capacity rapidly in contact with an aqueous medium again. Interestingly, the adhesiveness to wood was superior to strong commercial glues and, in addition, it could cause less environmental impact since it does not release toxic gasses in its application.

These interesting results, and considering the great diversity of polyelectrolytes and multivalent molecules available, opens a way to evaluate the behavior of other coacervates such as waterborne adhesives and glues.

**5.3.2. Biomimetic protocells.** Coacervates share some characteristics and functions with cellular organization, including liquid-liquid separation, confinement, compartmentalization, and catalytic properties.<sup>43,242–244</sup> In addition, the intracellular molecular crowding can be imitated and tuned by adding water-attracting and dehydrating additives (such as salt and polyethylene glycol) that allow increasing the effective concentration of the macromolecules in complex coacervates.<sup>245,246</sup> In parallel, advances in experimental techniques – in particular advanced microscopies – are making it possible to overcome the limitations when it comes to studying and quantifying complex coacervates both *in vitro* and *in vivo* conditions. In this framework, it is worth to highlight the tremendous advances in quantitative phase imaging (QPI), a powerful label-free wide-field microscopy approach to characterize

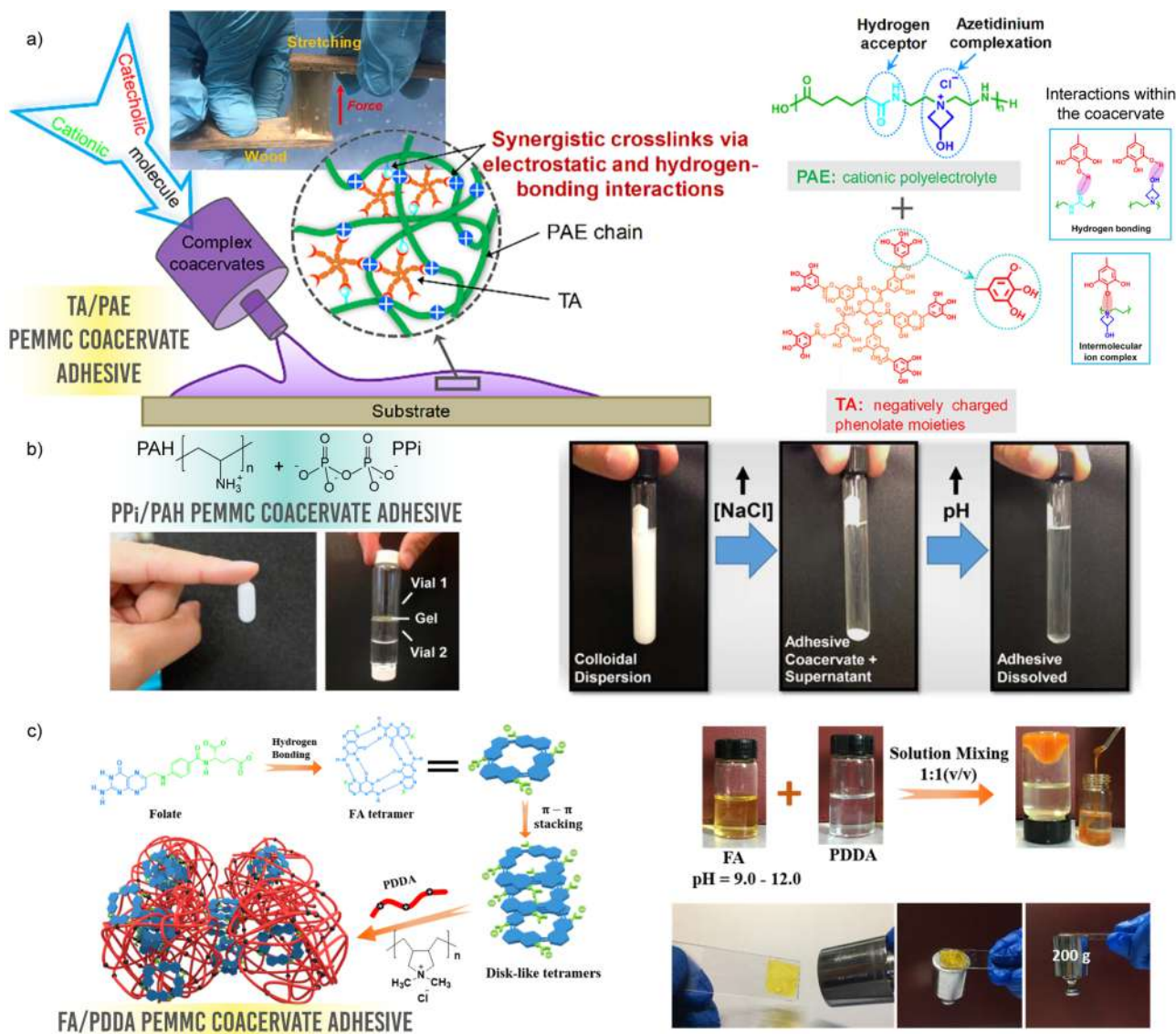


**Fig. 16** PEMMCs coacervates-based adhesives. (a) polyamidoamine/epichlorohydrin coacervates adhesive: schematic representation of the coacervate formation process, qualitative adhesive capacity and the non-covalent interactions that form the coacervate. Adapted and reproduced with permission from ref. 236 Copyright (2021) Elsevier. (b) polyallylamine/tripolyphosphate coacervates adhesives: qualitative adhesive capacity (left), coacervate formation with salt addition, and dissolution with pH increase (right). Adapted and reproduced with permission from ref. 119 and 240 Copyright (2014, 2015) American Chemical Society. (c) poly(diallyldimethylammonium)/folic acid quartet coacervate: schematic representation of the coacervate formation process, real image of the manufacturing process and qualitative adhesive capacity of a pre-dried coacervate sheet. Adapted and reproduced with permission from ref. 241 Copyright (2014) American Chemical Society.

and quantify (in real time) biomacromolecules in liquid condensates.<sup>247,248</sup>

For the reasons previously described, PECs have been postulated as membrane-free protocells or *in vitro* models to understand cellular processes and specific aspects of biogenesis.<sup>249,250</sup> In this framework, different types of coacervate-based protocells have been designed using bio-relevant building blocks such as peptides, polyamines, DNA and enzymes.<sup>43,141,146,251–253</sup> While most coacervates explored as protocells are formed by macromolecules, recently small metabolites have been evaluated as components too. Reversible compartmentalization as a result of coacervation between phosphate-containing nucleotides and

cationic peptides was explored in several reports.<sup>41,146,253</sup> Keating *et al.* studied the formation of PEMMC coacervates by combining polycations (poly-L-lysine and poly-arginine) and adenosine mono- ( $z = -2$ ), di- ( $z = -3$ ), and triphosphate ( $z = -4$ ) nucleotides (Fig. 17).<sup>25</sup> The properties of these protocells were compared with conventional coacervates formed using polymeric polyanions such as poly-D-glutamate and poly-DL-aspartate. Salt resistance, the provision of a distinctive microenvironment (local pH), prebiotic accumulation of RNA, and the effect on its structure were analyzed and compared for both types of designs. Interestingly, the PEMMC coacervates formed with multivalent anions generated different pH microenvironments, a higher capacity to

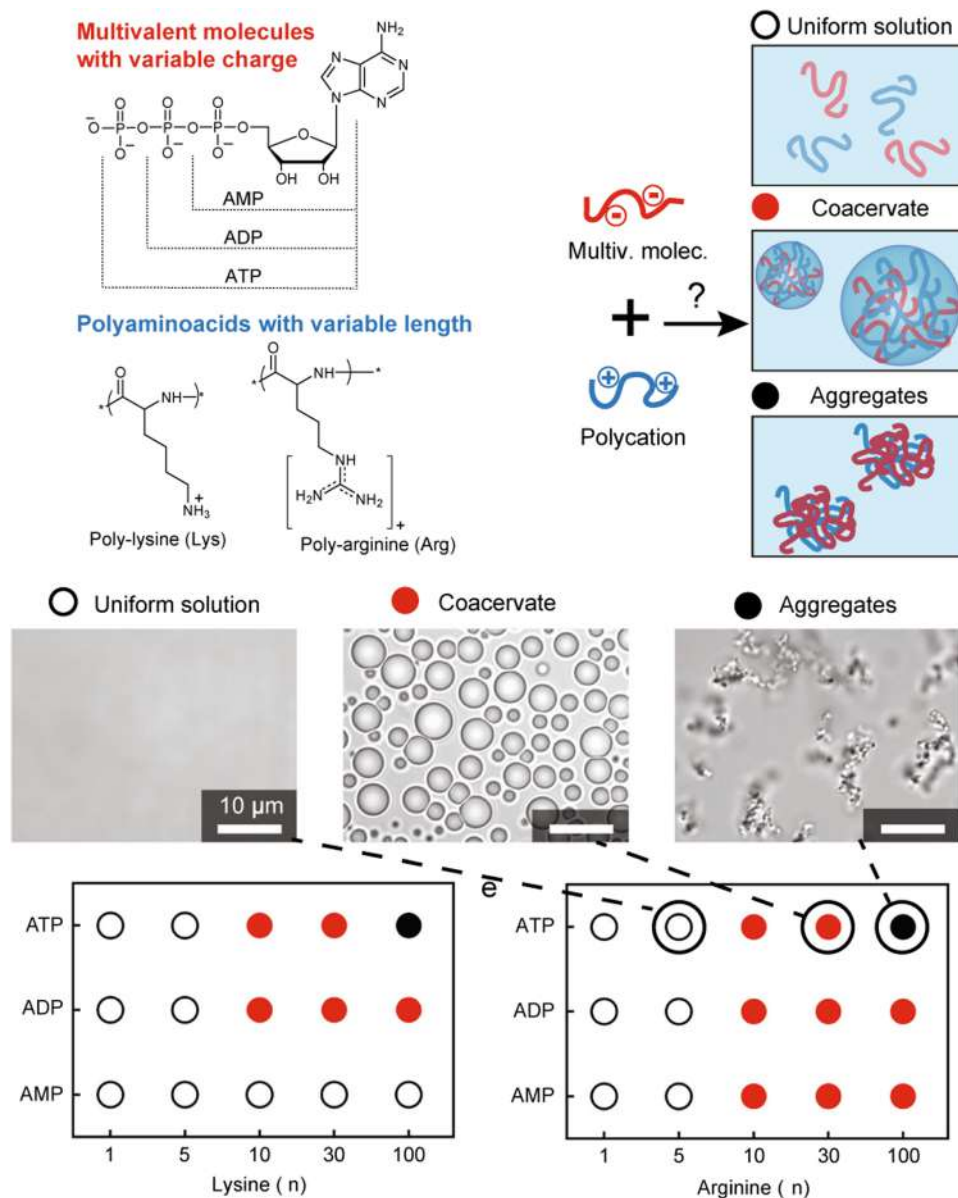


**Fig. 17** PEMMC-based protocells comprising lysine and arginine oligopeptides ( $n = 1$  to 100) and nucleotides with variable valency from  $z = -4$  (ATP) to  $z = -2$  (AMP): (top) structures of negatively and positively charged building blocks and a schematic representation of the formation of uniform solutions, coacervates and precipitates. The middle panel show optical microscope images illustrating samples categorized as uniform solution (white circles), coacervates (red circles) and aggregates (black circles); these particular samples are ATP with  $(\text{Arg})_n$  ( $n = 5, 30,$  and  $100$ , left-to-right), corresponding to the points highlighted in the panel below. While precipitates are prone to form using highly charged multivalent molecules combined with highly charged long oligocations, coacervates and uniform solutions are obtained when using poorly charged and short building blocks. Reproduced with permission from ref. 25 Copyright (2020) Springer Nature.

encapsulate and compartmentalize RNA, and a more effective preservation of RNA structure than those based on longer polyions. Therefore, these results indicate that PEMMCs can not only be postulated as functional compartments for prebiotic chemistry, but also may exhibit better properties as protocells than their higher molecular weight analogs. In another report, the same authors demonstrated that RNA can be combined with the oligoamines spermine ( $z = +4$ ) and spermidine ( $z = +3$ ) to form temperature-responsive coacervates with similar properties to peptide-based protocells in relation to compartmentalization and exchange capacities of relevant substrates.<sup>142</sup>

Spruijt *et al.* demonstrated that the formation and dissolution of the poly-L-lysine/ATP protocells can be fully controlled by changing the degree of phosphorylation of the multivalent molecule, applying an enzyme pair in the presence of certain bio-substrates (glucose and pyruvate).<sup>111</sup> Hexokinase activates coacervate formation in the presence of phosphoenolpyruvate, and then the dissolution of the system can occur in presence of pyroquinase and glucose as the second substrate. Recently, they exploited the conversion mechanism from ADP ( $z = -3$ ) to ATP ( $z = -4$ ) catalyzed by pyruvate kinase to control the formation of cationic fluorescent protein-containing K72/ATP coacervates.<sup>254</sup>

They showed that the droplets actively grow driven by the enzymatic reaction and, in addition, do not undergo aggregation processes, remaining stable for more than one hour.

Very recently, the same authors observed that a wide variety of small anionic metabolites (including multivalent anions based on sulfates, carboxylates, phosphates and redox species such as ferri- and ferrocyanides) can form complex coacervate protocells with a cationic peptide (oligoarginine).<sup>87</sup> Depending on the chemical composition, each system phase separates under different experimental conditions (concentration ratio and monovalent salt concentration). The differences in the phase behavior of each PEMMC system were exploited to

activate the formation or dissolution of coacervates by applying protometabolic chemical reactions. For example, the conversion of malonate and glyoxylate to 3-carboxymalate triggers the nucleation and steady growth of coacervate droplets (Fig. 18a). On the other hand, the oxidative decarboxylation of isocitroyl formate and aconitoyl formate by hydrogen peroxide leads to the loss of stability of the PEMMC coacervate and its consequent dissolution (Fig. 18b). In addition, by means of the NADH oxidation reaction, the authors showed that the coacervates with ferricyanide ions have the capacity to improve the yield of the reaction due to the internal confinement of the reagents.

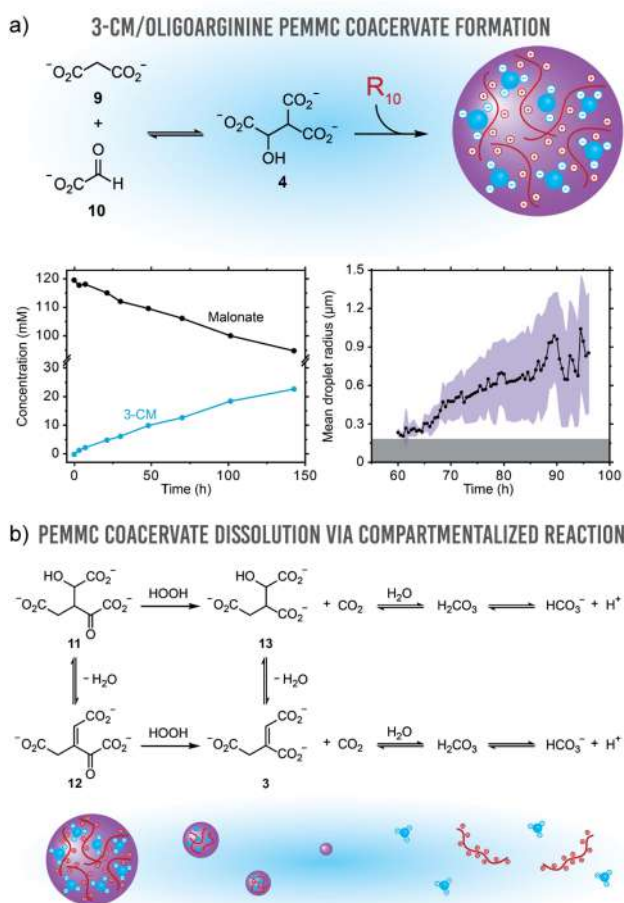


**Fig. 18** (a) Coacervate formation activated by Aldol addition reaction between malonate (9) ( $z = -2$ ) and glyoxylate (10) ( $z = -1$ ). The reaction generates 3-carboxymalate (3-CM, 4) which is able to act as a multivalent molecule ( $z = -3$ ) for the formation of an oligopeptide-based PEMMC. Plot of concentrations of malonate (black) and 3-CM (blue) over time for the reaction of 120 mM monosodium malonate with 120 mM sodium glyoxylate in the presence of 5 mM (Arg)<sub>10</sub> (R<sub>10</sub>) as observed by 1H-NMR spectroscopy (below, left) and analysis of droplet coacervate size over time (below, right). (b) Oxidative decarboxylation of isocitroyl formate and aconitoyl formate decreases coacervate stability. Isocitroyl formate (11) and aconitoyl formate (12) undergo oxidative decarboxylation by hydrogen peroxide (HOOH) to form isocitrate (13) and aconitate (3), respectively. Reproduced with permission from ref. 87 Copyright (2022) Wiley-VCH Verlag GmbH & Co.

## 6. Conclusion and perspectives

Polyelectrolyte complexes have become attractive soft materials from both scientific and technological perspectives. Although historically the main efforts have been focused on studying complexes formed between polymers of opposite charge (PECs), a considerable interest in single-polyelectrolyte platforms based on polymers complexed by small ionic molecules (PEMMCs) has emerged in the last few years for different technological purposes.<sup>255,256</sup> One of the main advantages of PEMMCs is their extremely simple, inexpensive and highly eco-friendly preparation process, since their synthesis does not require large amounts of toxic solvents, nor complex chemistry, nor large energy inputs. In addition, this architectural approach presents great versatility and flexibility due to the vast library of building blocks available that allow the generation of soft material with different macroscopic configurations (nanocomplexes, coacervates and films) and functionalities.

As described in the preceding sections, PEMMCs have shown attractive properties as functional soft materials in a wide spectrum of technological applications including: controlled drug release, functional films and coatings, eco-friendly glues and adhesives, and biomimetic protocells. However, compared to the application of complexes based on two polyelectrolytes, single polymer systems have been less applied, especially as coacervates and functional films. The latter, in conjunction with the great availability of construction scaffolds, opens the opportunity to continue designing increasingly efficient functional platforms.

In parallel, for the application of the systems to be consistent and successful, it is important to continue expanding the fundamental understanding of self-assembled complexes in all of their configurations. Compared to PECs, the basic physicochemical understanding of PEMMCs present significant gaps. Although PEMMCs have many similarities to PECs, in some respects they appear to exhibit different and unique behaviors and characteristics. This offers exciting opportunities to advance in new and fresh works that explore in depth the fundamental properties of PEMMCs using experimental and theoretical approaches. We believe that there is fertile ground to advance in studying different aspects of PEMMCs, such as: effect of pH, ionic strength and stoichiometry in the assembly process; effects

of identity, chemical sequence and topology of building blocks; effects of non-electrostatic interactions; stability over time of complexes; behavior and properties of ternary systems; among others. In addition to the basic studies based on conventional systems, it is necessary to broaden the physical-chemical exploration towards systems including biobased components, such as polysaccharides, proteins, peptides, biosurfactants, among others. The latter will allow reaching the basic understanding in more realistic systems.

Last but not least, we believe that for systems to go beyond the laboratory and result in useful technological applications for society, it may be useful to go deeper into the interdisciplinary exploration, study the possibilities of scaling industrially the most promising systems, and to work in collaboration with private technology companies.

## Conflicts of interest

There are no conflicts to declare.

## Acknowledgements

E. A. Acknowledges a scholarship from CONICET. W. A. M., and O. A. Acknowledge the financial support from Universidad Nacional de La Plata (PPID-X867), CONICET (PIP-0370), and ANPCyT (PICT-2017-1523, PICT2018-00780 and PICT2016-1680). S. E. H., M. L. A., M. L. C., W. M., M. T. and O. A. are CONICET fellows.

## References

- H. G. B. Jong and H. R. Kruyt, *Kolloid-Z.*, 1930, **50**, 39–48.
- H. L. Booij and H. G. Bungenberg de Jong, *Biocolloids and their Interactions*, Springer Vienna, Vienna, 1956, pp. 8–14.
- H. G. Bungenberg de Jong and H. R. Kruyt, *Proc. Sect. Sci. K. Ned. Akad. Wet.*, 1929, **32**, 849–856.
- H. G. Bungenberg de Jong, *Colloid Sci.*, 1949, **2**, 335–432.
- M. Muthukumar, *Macromolecules*, 2017, **50**, 9528–9560.
- S. Srivastava and M. V. Tirrell, *Adv. Chem. Phys.*, 2016, **161**, 499–544.
- F. W. Tiebackx, *Z. Chem. Ind. Kolloide*, 1911, **8**, 198–201.
- H. G. Bungenberg de Jong, *Colloid Sci.*, 1949, **2**, 232–258.
- B. Green and S. Lowell, *US Pat.*, 2,800,457, 1957.
- J. Fu and J. B. Schlenoff, *J. Am. Chem. Soc.*, 2016, **138**, 980–990.
- Q. Wang and J. B. Schlenoff, *Macromolecules*, 2014, **47**, 3108–3116.
- P. Schaaf and J. B. Schlenoff, *Adv. Mater.*, 2015, **27**, 2420–2432.
- R. F. Shamoun, A. Reisch and J. B. Schlenoff, *Adv. Funct. Mater.*, 2012, **22**, 1923–1931.
- L. Li, S. Srivastava, S. Meng, J. M. Ting and M. V. Tirrell, *Macromolecules*, 2020, **53**, 7835–7844.
- M. Yang, S. L. Sonawane, Z. A. Digby, J. G. Park and J. B. Schlenoff, *Macromolecules*, 2022, **55**, 7594–7604.
- A. E. Marras, J. M. Ting, K. C. Stevens and M. V. Tirrell, *J. Phys. Chem. B*, 2021, **125**, 7076–7089.
- Y. H. Kim, K. Lee and S. Li, *Chem. Mater.*, 2021, **33**, 7923–7943.
- M. J. Thiele, M. D. Davari, M. König, I. Hofmann, N. O. Junker, T. Mirzaei Garakani, L. Vojcic, J. Fitter and U. Schwaneberg, *ACS Catal.*, 2018, **8**, 10876–10887.
- S. Gao, A. Holkar and S. Srivastava, *Polymers*, 2019, **11**, 1097.
- S. Tabandeh and L. Leon, *Molecules*, 2019, **24**, 868.
- W. S. Cheow, T. Y. Kiew and K. Hadinoto, *Carbohydr. Polym.*, 2015, **117**, 549–558.
- M. Lueckheide, J. R. Vieregge, A. J. Bologna, L. Leon and M. V. Tirrell, *Nano Lett.*, 2018, **18**, 7111–7117.
- E. A. Frankel, P. C. Bevilacqua and C. D. Keating, *Langmuir*, 2016, **32**, 2041–2049.
- V. S. Meka, M. K. G. Sing, M. R. Pichika, S. R. Nali, V. R. M. Kolapalli and P. Kesharwani, *Drug Discov. Today*, 2017, **22**, 1697–1706.
- F. P. Cakmak, S. Choi, M. O. Meyer, P. C. Bevilacqua and C. D. Keating, *Nat. Commun.*, 2020, **11**, 5949.
- R. K. Rana, V. S. Murthy, J. Yu and M. S. Wong, *Adv. Mater.*, 2005, **17**, 1145–1150.
- Y. Lapitsky, *Curr. Opin. Colloid Interface Sci.*, 2014, **19**, 122–130.
- L. Zhou, H. Shi, Z. Li and C. He, *Macromol. Rapid Commun.*, 2020, **41**, 2000149.
- V. S. Murthy, R. K. Rana and M. S. Wong, *J. Phys. Chem. B*, 2006, **110**, 25619–25627.
- H. G. Bagaria and M. S. Wong, *J. Mater. Chem.*, 2011, **21**, 9454.
- Y. Lapitsky, *Curr. Opin. Colloid Interface Sci.*, 2014, **19**, 122–130.
- P. Calvo, C. Remuñán-López, J. L. Vila-Jato and M. J. Alonso, *J. Appl. Polym. Sci.*, 1997, **63**, 125–132.
- F. Rázga, D. Vnuková, V. Némethová, P. Mazancová and I. Lacík, *Carbohydr. Polym.*, 2016, **151**, 488–499.
- S. Hassani, A. Laouini, H. Fessi and C. Charcosset, *Colloids Surf., A*, 2015, **482**, 34–43.
- N. Sawtarie, Y. Cai and Y. Lapitsky, *Colloids Surf., B*, 2017, **157**, 110–117.
- Y. Huang and Y. Lapitsky, *J. Colloid Interface Sci.*, 2017, **486**, 27–37.
- Y. Cai and Y. Lapitsky, *J. Colloid Interface Sci.*, 2017, **494**, 242–254.
- M. Tirrell, *ACS Cent. Sci.*, 2018, **4**, 532–533.
- F. Comert, A. J. Malanowski, F. Azarikia and P. L. Dubin, *Soft Matter*, 2016, **12**, 4154–4161.
- K. A. Black, D. Priftis, S. L. Perry, J. Yip, W. Y. Byun and M. Tirrell, *ACS Macro Lett.*, 2014, **3**, 1088–1091.
- M. Abbas, W. P. Lipiński, J. Wang and E. Spruijt, *Chem. Soc. Rev.*, 2021, **50**, 3690–3705.
- W. C. Blocher McTigue and S. L. Perry, *Small*, 2020, **16**, 1907671.
- D. S. Williams, S. Koga, C. R. C. Hak, A. Majrekar, A. J. Patil, A. W. Perriman and S. Mann, *Soft Matter*, 2012, **8**, 6004.

- 44 J. T. King and A. Shakya, *Biophys J.*, 2021, **120**, 1139–1149.
- 45 R. Chollakup, J. B. Beck, K. Dirnberger, M. Tirrell and C. D. Eisenbach, *Macromolecules*, 2013, **46**, 2376–2390.
- 46 S. Meng, J. M. Ting, H. Wu and M. V. Tirrell, *Macromolecules*, 2020, **53**, 7944–7953.
- 47 A. B. Marciel, S. Srivastava and M. V. Tirrell, *Soft Matter*, 2018, **14**, 2454–2464.
- 48 J. R. Viereg, M. Lueckheide, A. B. Marciel, L. Leon, A. J. Bologna, J. R. Rivera and M. V. Tirrell, *J. Am. Chem. Soc.*, 2018, **140**, 1632–1638.
- 49 S. L. Perry, L. Leon, K. Q. Hoffmann, M. J. Kade, D. Priftis, K. A. Black, D. Wong, R. A. Klein, C. F. Pierce, K. O. Margossian, J. K. Whitmer, J. Qin, J. J. de Pablo and M. Tirrell, *Nat. Commun.*, 2015, **6**, 6052.
- 50 D. Priftis, R. Farina and M. Tirrell, *Langmuir*, 2012, **28**, 8721–8729.
- 51 D. S. Hwang, H. Zeng, A. Srivastava, D. V. Krogstad, M. Tirrell, J. N. Israelachvili and J. H. Waite, *Soft Matter*, 2010, **6**, 3232.
- 52 E. Spruijt, J. Sprakel, M. A. Cohen Stuart and J. van der Gucht, *Soft Matter*, 2010, **6**, 172–178.
- 53 K.-Y. Huang, H. Y. Yoo, Y. Jho, S. Han and D. S. Hwang, *ACS Nano*, 2016, **10**, 5051–5062.
- 54 Y. Jho, H. Y. Yoo, Y. Lin, S. Han and D. S. Hwang, *Adv. Colloid Interface Sci.*, 2017, **239**, 61–73.
- 55 Y. Zhang, P. Batys, J. T. O'Neal, F. Li, M. Sammalkorpi and J. L. Lutkenhaus, *ACS Cent. Sci.*, 2018, **4**, 638–644.
- 56 H. H. Hariri, A. M. Leahaf and J. B. Schlenoff, *Macromolecules*, 2012, **45**, 9364–9372.
- 57 E. Spruijt, A. H. Westphal, J. W. Borst, M. A. Cohen Stuart and J. van der Gucht, *Macromolecules*, 2010, **43**, 6476–6484.
- 58 J. van der Gucht, E. Spruijt, M. Lemmers and M. A. Cohen Stuart, *J. Colloid Interface Sci.*, 2011, **361**, 407–422.
- 59 M. Yang, Z. A. Digby and J. B. Schlenoff, *Macromolecules*, 2020, **53**, 5465–5474.
- 60 Z. A. Digby, M. Yang, S. Lteif and J. B. Schlenoff, *Macromolecules*, 2022, **55**, 978–988.
- 61 L. Li, S. Srivastava, M. Andreev, A. B. Marciel, J. J. de Pablo and M. V. Tirrell, *Macromolecules*, 2018, **51**, 2988–2995.
- 62 L. Li, A. M. Rumyantsev, S. Srivastava, S. Meng, J. J. de Pablo and M. V. Tirrell, *Macromolecules*, 2021, **54**, 105–114.
- 63 K. Sadman, Q. Wang, Y. Chen, B. Keshavarz, Z. Jiang and K. R. Shull, *Macromolecules*, 2017, **50**, 9417–9426.
- 64 M. Ghasemi and R. G. Larson, *AIChE J.*, 2022, **68**, e17646.
- 65 S. Chen and Z.-G. Wang, *Proc. Natl. Acad. Sci. U. S. A.*, 2022, **119**, e2209975119.
- 66 J. T. G. Overbeek and M. J. Voorn, *J. Cell. Comp. Physiol.*, 1957, **49**, 7–26.
- 67 I. Michaeli, J. T. G. Overbeek and M. J. Voorn, *J. Poly. Sci.*, 1957, **23**, 443–450.
- 68 A. Nakajima and H. Sato, *Biopolymers*, 1972, **11**, 1345–1355.
- 69 J. Qin, D. Priftis, R. Farina, S. L. Perry, L. Leon, J. Whitmer, K. Hoffmann, M. Tirrell and J. J. de Pablo, *ACS Macro Lett.*, 2014, **3**, 565–568.
- 70 C. E. Sing and S. L. Perry, *Soft Matter*, 2020, **16**, 2885–2914.
- 71 C. E. Sing, *Adv. Colloid Interface Sci.*, 2017, **239**, 2–16.
- 72 G. Debais and M. Tagliacucchi, *Macromolecules*, 2022, **55**, 5263–5275.
- 73 G. Debais and M. Tagliacucchi, *J. Chem. Phys.*, 2020, **153**, 144903.
- 74 A. Salehi and R. G. Larson, *Macromolecules*, 2016, **49**, 9706–9719.
- 75 J. Wang, M. A. Cohen Stuart and J. van der Gucht, *Macromolecules*, 2012, **45**, 8903–8909.
- 76 T. K. Lytle and C. E. Sing, *Soft Matter*, 2017, **13**, 7001–7012.
- 77 P. Zhang, N. M. Alsaifi, J. Wu and Z.-G. Wang, *J. Chem. Phys.*, 2018, **149**, 163303.
- 78 H. Eisenberg and G. R. Mohan, *J. Phys. Chem.*, 1959, **63**, 671–680.
- 79 P. Zhang, N. M. Alsaifi, J. Wu and Z.-G. Wang, *Macromolecules*, 2016, **49**, 9720–9730.
- 80 P. Zhang, K. Shen, N. M. Alsaifi and Z.-G. Wang, *Macromolecules*, 2018, **51**, 5586–5593.
- 81 S. Friedowitz, J. Lou, K. P. Barker, K. Will, Y. Xia and J. Qin, *Sci. Adv.*, 2021, **7**, eabg8654.
- 82 T. Zhu, Y. Sha, J. Yan, P. Pageni, M. A. Rahman, Y. Yan and C. Tang, *Nat Commun*, 2018, **9**, 4329.
- 83 E. V. Mechtaeva, I. M. Zorin, D. A. Gavrilova, P. A. Fetin, N. A. Zorina and A. Yu. Bilibin, *J. Mol Liq*, 2019, **293**, 111418.
- 84 S. E. Herrera, M. L. Agazzi, M. L. Cortez, W. A. Marmisollé, M. Tagliacucchi and O. Azzaroni, *ChemPhysChem*, 2019, **20**, 1044–1053.
- 85 Y. Huang and Y. Lapitsky, *J. Colloid Interface Sci*, 2017, **486**, 27–37.
- 86 J. Pelta, F. Livolant and J.-L. Sikorav, *J. Biol. Chem.*, 1996, **271**, 5656–5662.
- 87 I. B. A. Smokers, M. H. I. van Haren, T. Lu and E. Spruijt, *ChemSystemsChem*, 2022, **4**, e20220000.
- 88 S. Chen, P. Zhang and Z.-G. Wang, *Macromolecules*, 2022, **55**, 3898–3909.
- 89 S. Pistone, D. Qoragllu, G. Smistad and M. Hiorth, *Soft Matter*, 2015, **11**, 5765–5774.
- 90 Y. Yang, J. Cheng, V. M. Garamus, N. Li and A. Zou, *J. Agric. Food Chem.*, 2018, **66**, 1067–1074.
- 91 T. López-León, E. L. S. Carvalho, B. Seijo, J. L. Ortega-Vinuesa and D. Bastos-González, *J. Colloid Interface Sci*, 2005, **283**, 344–351.
- 92 Y. Cai and Y. Lapitsky, *Colloids Surf., B*, 2020, **193**, 111081.
- 93 F. M. Goycoolea, G. Lollo, C. Remuñán-López, F. Quaglia and M. J. Alonso, *Biomacromolecules*, 2009, **10**, 1736–1743.
- 94 F. Furlani, P. Parisse and P. Sacco, *Molecules*, 2020, **25**, 1071.
- 95 Y. Zhang, E. Yildirim, H. S. Antila, L. D. Valenzuela, M. Sammalkorpi and J. L. Lutkenhaus, *Soft Matter*, 2015, **11**, 7392–7401.
- 96 E. Guzmán, L. Fernández-Peña, F. Ortega and R. G. Rubio, *Curr. Opin. Colloid Interface Sci.*, 2020, **48**, 91–108.
- 97 B. J. McKenna, H. Birkedal, M. H. Bartl, T. J. Deming and G. D. Stucky, *Angew. Chem., Int. Ed.*, 2004, **43**, 5652–5655.
- 98 Y. Huang and Y. Lapitsky, *J. Phys. Chem. B*, 2013, **117**, 9548–9557.

- 99 W. S. Cheow and K. Hadinoto, *Langmuir*, 2012, **28**, 6265–6275.
- 100 F. Atyabi and R. Dinarvand, *Int. J. Nanomedicine*, 2011, 1487.
- 101 W. S. Cheow and K. Hadinoto, *Colloids Surf., B*, 2012, **92**, 55–63.
- 102 M.-H. Nguyen, T.-T. Tran and K. Hadinoto, *Eur. J. Pharm. Biopharm.*, 2016, **104**, 156–163.
- 103 W. S. Cheow, T. Y. Kiew, Y. Yang and K. Hadinoto, *Mol Pharm*, 2014, **11**, 1611–1620.
- 104 D. Hassan, C. A. Omolo, R. Gannimani, A. Y. Waddad, C. Mocktar, S. Rambharose, N. Agrawal and T. Govender, *Int. J. Pharm.*, 2019, **558**, 143–156.
- 105 B. Dong and K. Hadinoto, *Int. J. Biol. Macromol.*, 2019, **139**, 500–508.
- 106 M. H. Nguyen, H. Yu, T. Y. Kiew and K. Hadinoto, *Eur. J. Pharm. Biopharm.*, 2015, **96**, 1–10.
- 107 B. Dong and K. Hadinoto, *Drug Dev Ind Pharm*, 2017, **43**, 996–1002.
- 108 D. R. Sikwal, R. S. Kalhapure, S. Rambharose, S. Vepuri, M. Soliman, C. Mocktar and T. Govender, *Mater. Sci. Eng., C*, 2016, **63**, 489–498.
- 109 M. Yang, Z. A. Digby, Y. Chen and J. B. Schlenoff, *Sci. Adv.*, 2022, **8**, eabm4783.
- 110 J. Zhou, M. Barz and F. Schmid, *J. Chem. Phys.*, 2016, **144**, 164902.
- 111 K. K. Nakashima, J. F. Baaij and E. Spruijt, *Soft Matter*, 2018, **14**, 361–367.
- 112 J. Wang, M. Abbas, J. Wang and E. Spruijt, *ChemRxiv*.
- 113 G. Laucirica, W. A. Marmisollé and O. Azzaroni, *Phys. Chem. Chem. Phys.*, 2017, **19**, 8612–8620.
- 114 V. S. Rathee, A. J. Zervoudakis, H. Sidky, B. J. Sikora and J. K. Whitmer, *J. Chem. Phys.*, 2018, **148**, 114901.
- 115 J. Th and G. Overbeek, *Bull. Soc. Chim. Belg.*, 2010, **57**, 252–261.
- 116 A. Katchalsky, *Biophys J.*, 1964, **4**, 9–41.
- 117 A. I. Petrov, A. A. Antipov and G. B. Sukhorukov, *Macromolecules*, 2003, **36**, 10079–10086.
- 118 S. E. Herrera, M. L. Agazzi, M. L. Cortez, W. A. Marmisollé, M. Tagliazucchi and O. Azzaroni, *Phys. Chem. Chem. Phys.*, 2020, **22**, 7440–7450.
- 119 P. G. Lawrence and Y. Lapitsky, *Langmuir*, 2015, **31**, 1564–1574.
- 120 T. Lu, K. K. Nakashima and E. Spruijt, *J. Phys. Chem. B*, 2021, **125**, 3080–3091.
- 121 S. E. Herrera, M. L. Agazzi, M. L. Cortez, W. A. Marmisollé, M. Tagliazucchi and O. Azzaroni, *Chem. Commun.*, 2019, **55**, 14653–14656.
- 122 M. Delsanti, J. P. Dalbiez, O. Spalla, L. Belloni and M. Drifford, *ACS Symp. Ser.*, 1993, **548**, 381–392.
- 123 L. Belloni, M. Olvera de la Cruz, M. Delsanti, J. P. Dalbiez, O. Spalla and M. Drifford, *Il Nuovo Cimento D*, 1994, vol. 16, pp. 727–736.
- 124 E. Raspaud, M. Olvera de la Cruz, J.-L. Sikorav and F. Livolant, *Biophys J.*, 1998, **74**, 381–393.
- 125 I. Sabbagh and M. Delsanti, *Eur. Phys. J. E: Soft Matter*, 2000, **1**, 75–86.
- 126 A. Escobar, N. E. Muzzio, P. Andreozzi, S. Libertone, E. Tasca, O. Azzaroni, M. Grzelczak and S. E. Moya, *Adv. Mater. Interfaces*, 2019, **6**, 1901373.
- 127 B. C. Hoopes and W. R. McClure, *Nucleic Acids Res.*, 1981, **9**, 5493–5504.
- 128 K. Besteman, K. van Eijk and S. G. Lemay, *Nat. Phys.*, 2007, **3**, 641–644.
- 129 Y. Burak, G. Ariel and D. Andelman, *Biophys J.*, 2003, **85**, 2100–2110.
- 130 F. J. Solis and M. Olvera de laCruz, *Eur. Phys. J. E: Soft Matter Biol. Phys.*, 2001, **4**, 143–152.
- 131 Y. Hayashi, M. Ullner and P. Linse, *J. Phys. Chem. B*, 2003, **107**, 8198–8207.
- 132 E. Meneses-Juárez, C. Márquez-Beltrán, J. F. Rivas-Silva, U. Pal and M. González-Melchor, *Soft Matter*, 2015, **11**, 5889–5897.
- 133 Y. Hayashi, M. Ullner and P. Linse, *J. Chem. Phys.*, 2002, **116**, 6836–6845.
- 134 Y. Hayashi, M. Ullner and P. Linse, *J. Phys. Chem. B*, 2004, **108**, 15266–15277.
- 135 K. Besteman, K. van Eijk and S. G. Lemay, *Nat. Phys.*, 2007, **3**, 641–644.
- 136 A. Shakya, M. Girard, J. T. King and M. Olvera de la Cruz, *Macromolecules*, 2020, **53**, 1258–1269.
- 137 A. Shakya and J. T. King, *Biophys J.*, 2018, **115**, 1840–1847.
- 138 Y. Yuan and Y. Huang, *Soft Matter*, 2019, **15**, 9871–9880.
- 139 R. Zhang and B. I. Shklovskii, *Phys. A*, 2005, **352**, 216–238.
- 140 P. Andreozzi, C. Ricci, J. E. M. Porcel, P. Moretti, D. di Silvio, H. Amenitsch, M. G. Ortore and S. E. Moya, *J. Colloid Interface Sci.*, 2019, **543**, 335–342.
- 141 R. R. Poudyal, F. Pir Cakmak, C. D. Keating and P. C. Bevilacqua, *Biochemistry*, 2018, **57**, 2509–2519.
- 142 W. M. Aumiller, F. Pir Cakmak, B. W. Davis and C. D. Keating, *Langmuir*, 2016, **32**, 10042–10053.
- 143 V. E. Cuenca, H. Martinelli, M. A. Ramirez, H. A. Ritacco, P. Andreozzi and S. E. Moya, *Langmuir*, 2019, **35**, 14300–14309.
- 144 H. Kim, B. Jeon, S. Kim, Y. Jho and D. S. Hwang, *Polymers*, 2019, **11**, 691.
- 145 Y. Kang, C. Wang, K. Liu, Z. Wang and X. Zhang, *Langmuir*, 2012, **28**, 14562–14566.
- 146 W. M. Aumiller and C. D. Keating, *Nat Chem*, 2016, **8**, 129–137.
- 147 P. G. Lawrence and Y. Lapitsky, *Langmuir*, 2015, **31**, 1564–1574.
- 148 W. C. Blocher and S. L. Perry, *WIREs Nanomedicine and Nanobiotechnology*, 2017, **9**, e1442.
- 149 W. C. Blocher McTigue and S. L. Perry, *Soft Matter*, 2019, **15**, 3089–3103.
- 150 D. di Silvio, M. Martínez-Moro, C. Salvador, M. de los Angeles Ramirez, P. R. Caceres-Velez, M. G. Ortore, D. Dupin, P. Andreozzi and S. E. Moya, *J. Colloid Interface Sci.*, 2019, **557**, 757–766.
- 151 Z. W. Lim, Y. Ping and A. Miserez, *Bioconjugate Chem.*, 2018, **29**, 2176–2180.
- 152 A. Farashishiko, S. E. Plush, K. B. Maier, A. Dean Sherry and M. Woods, *Chem. Commun.*, 2017, **53**, 6355–6358.

- 153 N. Choudhury, M. Meghwal and K. Das, *Food Front.*, 2021, **2**, 426–442.
- 154 M. Zhao and N. S. Zacharia, *J. Chem. Phys.*, 2018, **149**, 163326.
- 155 Z. Jiang, J. Chen, L. Cui, X. Zhuang, J. Ding and X. Chen, *Small Methods*, 2018, **2**, 1700307.
- 156 X. An, A. Zhu, H. Luo, H. Ke, H. Chen and Y. Zhao, *ACS Nano*, 2016, **10**, 5947–5958.
- 157 Z. Yang, L. Chen, D. J. McClements, C. Qiu, C. Li, Z. Zhang, M. Miao, Y. Tian, K. Zhu and Z. Jin, *Food Hydrocolloids*, 2022, **124**, 107218.
- 158 P. Andreozzi, E. Diamanti, K. R. Py-Daniel, P. R. Cáceres-Vélez, C. Martinelli, N. Politakos, A. Escobar, M. Muzi-Falconi, R. Azevedo and S. E. Moya, *ACS Appl. Mater. Interfaces*, 2017, **9**, 38242–38254.
- 159 N. A. Bakh, A. B. Cortinas, M. A. Weiss, R. S. Langer, D. G. Anderson, Z. Gu, S. Dutta and M. S. Strano, *Nat. Chem.*, 2017, **9**, 937–944.
- 160 J. Xie, A. Li and J. Li, *Macromol. Rapid Commun.*, 2017, **38**, 1700413.
- 161 M. J. Webber and D. G. Anderson, *J. Drug Targeting*, 2015, **23**, 651–655.
- 162 Z. Gu, T. T. Dang, M. Ma, B. C. Tang, H. Cheng, S. Jiang, Y. Dong, Y. Zhang and D. G. Anderson, *ACS Nano*, 2013, **7**, 6758–6766.
- 163 M. A. VandenBerg and M. J. Webber, *Adv. Healthcare Mater.*, 2019, **8**, 1801466.
- 164 M. L. Agazzi, S. E. Herrera, M. L. Cortez, W. A. Marmisollé, M. Tagliazucchi and O. Azzaroni, *Chem. – Eur. J.*, 2020, **26**, 2456–2463.
- 165 Q. Hu, P. S. Katti and Z. Gu, *Nanoscale*, 2014, **6**, 12273–12286.
- 166 R. de la Rica, D. Aili and M. M. Stevens, *Adv. Drug Delivery Rev.*, 2012, **64**, 967–978.
- 167 I. Insua, M. Petit, L. D. Blackman, R. Keogh, A. Pitto-Barry, R. K. O'Reilly, A. F. A. Peacock, A. M. Krachler and F. Fernandez-Trillo, *ChemNanoMat*, 2018, **4**, 807–814.
- 168 I.-C. Sun, H. Y. Yoon, D.-K. Lim and K. Kim, *Bioconjugate Chem.*, 2020, **31**, 1012–1024.
- 169 M. Shahriari, M. Zahiri, K. Abnous, S. M. Taghdisi, M. Ramezani and M. Alibolandi, *J. Controlled Release*, 2019, **308**, 172–189.
- 170 A. Kumari, K. Kumari and S. Gupta, *Sci. Rep.*, 2019, **9**, 20334.
- 171 M. L. Agazzi, S. E. Herrera, M. L. Cortez, W. A. Marmisollé and O. Azzaroni, *Colloids Surf., B*, 2020, **190**, 110895.
- 172 Y. Wang, Y. Deng, H. Luo, A. Zhu, H. Ke, H. Yang and H. Chen, *ACS Nano*, 2017, **11**, 12134–12144.
- 173 J. Borges, L. C. Rodrigues, R. L. Reis and J. F. Mano, *Adv. Funct. Mater.*, 2014, **24**, 5624–5648.
- 174 M. Molina, S. Wedepohl and M. Calderón, *Nanoscale*, 2016, **8**, 5852–5856.
- 175 J. M. Giussi, M. I. Velasco, G. S. Longo, R. H. Acosta and O. Azzaroni, *Soft Matter*, 2015, **11**, 8879–8886.
- 176 A. Bordat, T. Boissenot, J. Nicolas and N. Tsapis, *Adv. Drug Delivery Rev.*, 2019, **138**, 167–192.
- 177 D. Fernández-Quiroz, Á. González-Gómez, J. Lizardi-Mendoza, B. Vázquez-Lasa, F. M. Goycoolea, J. San Román and W. M. Argüelles-Monal, *Carbohydr. Polym.*, 2015, **134**, 92–101.
- 178 J. Bergueiro and M. Calderón, *Macromol. Biosci.*, 2015, **15**, 183–199.
- 179 N. S. Rejinold, K. P. Chennazhi, S. V. Nair, H. Tamura and R. Jayakumar, *Carbohydr. Polym.*, 2011, **83**, 776–786.
- 180 M. Karimi, P. Sahandi Zangabad, A. Ghasemi, M. Amiri, M. Bahrami, H. Malekzad, H. Ghahramanzadeh Asl, Z. Mahdieh, M. Bozorgomid, A. Ghasemi, M. R. Rahmani Taji Boyuk and M. R. Hamblin, *ACS Appl. Mater. Interfaces*, 2016, **8**, 21107–21133.
- 181 J. M. Giussi, C. von Bilderling, E. Alarcón, L. I. Pietrasanta, R. Hernandez, R. P. del Real, M. Vázquez, C. Mijangos, M. L. Cortez and O. Azzaroni, *Nanoscale*, 2018, **10**, 1189–1195.
- 182 Y. Zhou, H. Ye, Y. Chen, R. Zhu and L. Yin, *Biomacromolecules*, 2018, **19**, 1840–1857.
- 183 D. Fernández-Quiroz, J. Loya-Duarte, E. Silva-Campa, W. Argüelles-Monal, A. Sarabia-Sainz, A. Lucero-Acuña, T. del Castillo-Castro, J. San Román, J. Lizardi-Mendoza, A. J. Burgara-Estrella, B. Castaneda, D. Soto-Puebla and M. Pedroza-Montero, *J. Appl. Polym. Sci.*, 2019, **136**, 47831.
- 184 H. Horo, S. Das, B. Mandal and L. M. Kundu, *Int. J. Biol. Macromol.*, 2019, **121**, 1070–1076.
- 185 N. Devi, M. Sarmah, B. Khatun and T. K. Maji, *Adv. Colloid Interface Sci.*, 2017, **239**, 136–145.
- 186 B. Muhoza, S. Xia, X. Wang, X. Zhang, Y. Li and S. Zhang, *Crit. Rev. Food Sci. Nutr.*, 2022, **62**, 1363–1382.
- 187 Y. P. Timilsena, T. O. Akanbi, N. Khalid, B. Adhikari and C. J. Barrow, *Int. J. Biol. Macromol.*, 2019, **121**, 1276–1286.
- 188 J. L. Muriel Mundo, J. Liu, Y. Tan, H. Zhou, Z. Zhang and D. J. McClements, *Food Res. Int.*, 2020, **128**, 108781.
- 189 P. G. Lawrence, P. S. Patil, N. D. Leipzig and Y. Lapitsky, *ACS Appl. Mater. Interfaces*, 2016, **8**, 4323–4335.
- 190 U. K. de Silva, J. L. Brown and Y. Lapitsky, *RSC Adv.*, 2018, **8**, 19409–19419.
- 191 S. S. Alam, Y. Seo and Y. Lapitsky, *ACS Appl. Bio. Mater.*, 2020, **3**, 8427–8437.
- 192 S. S. Alam, C. B. Mather, Y. Seo and Y. Lapitsky, *Colloids Surf., A*, 2021, **629**, 127490.
- 193 J. J. Richardson, J. Cui, M. Björnmalm, J. A. Braunger, H. Ejima and F. Caruso, *Chem. Rev.*, 2016, **116**, 14828–14867.
- 194 S. Zhao, F. Caruso, L. Dähne, G. Decher, B. G. de Geest, J. Fan, N. Feliu, Y. Gogotsi, P. T. Hammond, M. C. Hersam, A. Khademhosseini, N. Kotov, S. Leporatti, Y. Li, F. Lisdat, L. M. Liz-Marzán, S. Moya, P. Mulvaney, A. L. Rogach, S. Roy, D. G. Shchukin, A. G. Skirtach, M. M. Stevens, G. B. Sukhorukov, P. S. Weiss, Z. Yue, D. Zhu and W. J. Parak, *ACS Nano*, 2019, **13**, 6151–6169.
- 195 J. J. Richardson, J. Cui, M. Björnmalm, J. A. Braunger, H. Ejima and F. Caruso, *Chem. Rev.*, 2016, **116**, 14828–14867.
- 196 A. Escobar, N. Muzzio and S. E. Moya, *Pharmaceutics*, 2020, **13**, 16.

- 197 L. Séon, P. Lavalle, P. Schaaf and F. Boulmedais, *Langmuir*, 2015, **31**, 12856–12872.
- 198 A. Salehi, P. S. Desai, J. Li, C. A. Steele and R. G. Larson, *Macromolecules*, 2015, **48**, 400–409.
- 199 G. Debais and M. Tagliazucchi, *Macromolecules*, 2022, **55**, 5263–5275.
- 200 S. E. Herrera, M. L. Agazzi, M. L. Cortez, W. A. Marmisollé, C. Bilderling and O. Azzaroni, *Macromol. Chem. Phys.*, 2019, **220**, 1900094.
- 201 J. Irigoyen, S. E. Moya, J. J. Iturri, I. Llerena, O. Azzaroni and E. Donath, *Langmuir*, 2009, **25**, 3374–3380.
- 202 N. E. Muzzio, M. A. Pasquale, E. Diamanti, D. Gregurec, M. M. Moro, O. Azzaroni and S. E. Moya, *Mater. Sci. Eng. C*, 2017, **80**, 677–687.
- 203 N. E. Muzzio, D. Gregurec, E. Diamanti, J. Irigoyen, M. A. Pasquale, O. Azzaroni and S. E. Moya, *Adv. Mater. Interfaces*, 2017, **4**, 1600126.
- 204 I. S. Kurtz, S. Sui, X. Hao, M. Huang, S. L. Perry and J. D. Schiffman, *ACS Appl. Bio Mater.*, 2019, **2**, 3926–3933.
- 205 V. Ball, M. Michel, V. Toniazzo and D. Ruch, *Ind. Eng. Chem. Res.*, 2013, **52**, 5691–5699.
- 206 N. E. Muzzio, M. A. Pasquale, W. A. Marmisollé, C. von Bilderling, M. L. Cortez, L. I. Pietrasanta and O. Azzaroni, *Biomater. Sci.*, 2018, **6**, 2230–2247.
- 207 R. J. Smith, C. T. Long and J. C. Grunlan, *Langmuir*, 2018, **34**, 11086–11091.
- 208 H.-C. Chiang, B. Eberle, D. Carlton, T. J. Kolibaba and J. C. Grunlan, *ACS Food Sci. Technol.*, 2021, **1**, 495–499.
- 209 M. Haile, O. Sarwar, R. Henderson, R. Smith and J. C. Grunlan, *Macromol. Rapid Commun.*, 2017, **38**, 1600594.
- 210 W. A. Marmisollé, J. Irigoyen, D. Gregurec, S. Moya and O. Azzaroni, *Adv. Funct. Mater.*, 2015, **25**, 4144–4152.
- 211 M. L. Agazzi, S. E. Herrera, M. L. Cortez, W. A. Marmisollé, C. von Bilderling, L. I. Pietrasanta and O. Azzaroni, *Soft Matter*, 2019, **15**, 1640–1650.
- 212 J. Yang, L. Xiong, M. Li and Q. Sun, *J. Agric. Food Chem.*, 2018, **66**, 6104–6115.
- 213 R. F. Shamoun, H. H. Hariri, R. A. Ghostine and J. B. Schlenoff, *Macromolecules*, 2012, **45**, 9759–9767.
- 214 K. D. Kelly and J. B. Schlenoff, *ACS Appl. Mater. Interfaces*, 2015, **7**, 13980–13986.
- 215 R. R. Costa, A. M. S. Costa, S. G. Caridade and J. F. Mano, *Chem. Mater.*, 2015, **27**, 7490–7502.
- 216 M. N. Rodrigues, M. B. Oliveira, R. R. Costa and J. F. Mano, *Biomacromolecules*, 2016, **17**, 2178–2188.
- 217 M. Matsuo and K. Kurihara, *Nat. Commun.*, 2021, **12**, 5487.
- 218 X. Zhang, Y. Lin, N. A. Eschmann, H. Zhou, J. N. Rauch, I. Hernandez, E. Guzman, K. S. Kosik and S. Han, *PLoS Biol.*, 2017, **15**, e2002183.
- 219 Y. Lin, J. McCarty, J. N. Rauch, K. T. Delaney, K. S. Kosik, G. H. Fredrickson, J.-E. Shea and S. Han, *Elife*, 2019, **8**, e42571.
- 220 H. Zhao, C. Sun, R. J. Stewart and J. H. Waite, *J. Biol. Chem.*, 2005, **280**, 42938–42944.
- 221 S. Kim, J. Huang, Y. Lee, S. Dutta, H. Y. Yoo, Y. M. Jung, Y. Jho, H. Zeng and D. S. Hwang, *Proc. Natl. Acad. Sci. U. S. A.*, 2016, **113**, E847–E853.
- 222 S. Kim, H. Y. Yoo, J. Huang, Y. Lee, S. Park, Y. Park, S. Jin, Y. M. Jung, H. Zeng, D. S. Hwang and Y. Jho, *ACS Nano*, 2017, **11**, 6764–6772.
- 223 D. S. Hwang, J. H. Waite and M. Tirrell, *Biomaterials*, 2010, **31**, 1080–1084.
- 224 Y. Zhao, Y. Wu, L. Wang, M. Zhang, X. Chen, M. Liu, J. Fan, J. Liu, F. Zhou and Z. Wang, *Nat. Commun.*, 2017, **8**, 2218.
- 225 A. H. Hofman, I. A. van Hees, J. Yang and M. Kamperman, *Adv. Mater.*, 2018, **30**, 1704640.
- 226 R. J. Stewart, C. S. Wang and H. Shao, *Adv. Colloid Interface Sci.*, 2011, **167**, 85–93.
- 227 C. Heinzmann, C. Weder and L. M. de Espinosa, *Chem. Soc. Rev.*, 2016, **45**, 342–358.
- 228 J. Saiz-Poseu, J. Mancebo-Aracil, F. Nador, F. Busqué and D. Ruiz-Molina, *Angew. Chem., Int. Ed.*, 2019, **58**, 696–714.
- 229 W. Zhang, R. Wang, Z. Sun, X. Zhu, Q. Zhao, T. Zhang, A. Cholewinski, F. (Kuo) Yang, B. Zhao, R. Pinnaratip, P. K. Forooshani and B. P. Lee, *Chem. Soc. Rev.*, 2020, **49**, 433–464.
- 230 Q. Zhao, D. W. Lee, B. K. Ahn, S. Seo, Y. Kaufman, J. N. Israelachvili and J. H. Waite, *Nat. Mater.*, 2016, **15**, 407–412.
- 231 X. Wei, K. Ma, Y. Cheng, L. Sun, D. Chen, X. Zhao, H. Lu, B. Song, K. Yang and P. Jia, *ACS Appl. Polym. Mater.*, 2020, **2**, 2541–2549.
- 232 X. Wei, D. Chen, X. Zhao, J. Luo, H. Wang and P. Jia, *ACS Appl. Polym. Mater.*, 2021, **3**, 837–846.
- 233 B. Reis, D. Vehlow, T. Rust, D. Kuckling and M. Müller, *Int. J. Mol. Sci.*, 2019, **20**, 6081.
- 234 J. Ren, R. Kong, Y. Gao, L. Zhang and J. Zhu, *J. Colloid Interface Sci.*, 2021, **602**, 406–414.
- 235 H. Fan, J. Wang, Q. Zhang and Z. Jin, *ACS Omega*, 2017, **2**, 6668–6676.
- 236 Z. Wang, S. Zhang, S. Zhao, H. Kang, Z. Wang, C. Xia, Y. Yu and J. Li, *Chem. Eng. J.*, 2021, **404**, 127069.
- 237 M. Vahdati, F. J. Cedano-Serrano, C. Creton and D. Hourdet, *ACS Appl. Polym. Mater.*, 2020, **2**, 3397–3410.
- 238 M. Dompé, M. Vahdati, F. van Ligten, F. J. Cedano-Serrano, D. Hourdet, C. Creton, M. Zanetti, P. Bracco, J. van der Gucht, T. Kodger and M. Kamperman, *ACS Appl. Polym. Mater.*, 2020, **2**, 1722–1730.
- 239 Q. Peng, Q. Wu, J. Chen, T. Wang, M. Wu, D. Yang, X. Peng, J. Liu, H. Zhang and H. Zeng, *ACS Appl. Mater. Interfaces*, 2021, **13**, 48239–48251.
- 240 Y. Huang, P. G. Lawrence and Y. Lapitsky, *Langmuir*, 2014, **30**, 7771–7777.
- 241 S. Gao, W. Wang, T. Wu, S. Jiang, J. Qi, Z. Zhu, B. Zhang, J. Huang and Y. Yan, *ACS Appl. Mater. Interfaces*, 2021, **13**, 34843–34850.
- 242 S. Alberti, A. Gladfelter and T. Mittag, *Cell*, 2019, **176**, 419–434.
- 243 T. Lu and E. Spruijt, *J. Am. Chem. Soc.*, 2020, **142**, 2905–2914.
- 244 K. Lv, A. W. Perriman and S. Mann, *Chem. Commun.*, 2015, **51**, 8600–8602.
- 245 S. Park, R. Barnes, Y. Lin, B. Jeon, S. Najafi, K. T. Delaney, G. H. Fredrickson, J.-E. Shea, D. S. Hwang and S. Han, *Commun. Chem.*, 2020, **3**, 83.

- 246 Y. Hong, S. Najafi, T. Casey, J.-E. Shea, S.-I. Han and D. S. Hwang, *Nat. Commun.*, 2022, **13**, 7326.
- 247 Y. Hong, K. P. Dao, T. Kim, S. Lee, Y. Shin, Y. Park and D. S. Hwang, *Adv. Opt. Mater.*, 2021, **9**, 2100697.
- 248 T. L. Nguyen, S. Pradeep, R. L. Judson-Torres, J. Reed, M. A. Teitell and T. A. Zangle, *ACS Nano*, 2022, **16**, 11516–11544.
- 249 N. A. Yewdall, A. A. M. André, T. Lu and E. Spruijt, *Curr. Opin. Colloid Interface Sci.*, 2021, **52**, 101416.
- 250 M. Matsuo and K. Kurihara, *Nat. Commun.*, 2021, **12**, 5487.
- 251 S. Koga, D. S. Williams, A. W. Perriman and S. Mann, *Nat. Chem.*, 2011, **3**, 720–724.
- 252 T. Lu, S. Liese, L. Schoenmakers, C. A. Weber, H. Suzuki, W. T. S. Huck and E. Spruijt, *J. Am. Chem. Soc.*, 2022, **144**, 13451–13455.
- 253 M. Abbas, W. P. Lipiński, K. K. Nakashima, W. T. S. Huck and E. Spruijt, *Nat. Chem.*, 2021, **13**, 1046–1054.
- 254 K. K. Nakashima, M. H. I. van Haren, A. A. M. André, I. Robu and E. Spruijt, *Nat. Commun.*, 2021, **12**, 3819.
- 255 G. Pérez-Mitta, W. A. Marmisollé, A. G. Albesa, M. E. Toimil-Molares, C. Trautmann and O. Azzaroni, *Small*, 2018, **14**, 1702131.
- 256 G. Laucirica, G. Pérez-Mitta, M. E. Toimil-Molares, C. Trautmann, W. A. Marmisollé and O. Azzaroni, *J. Phys. Chem. C*, 2019, **123**, 28997–29007.